EFFECT OF GIRDER SPACING ON THE CONSTRUCTION COST AND SEISMIC PERFORMANCE OF SLAB-ON-PRESTRESSED CONCRETE GIRDER HIGHWAY BRIDGES

A THESIS SUBMITTED TO
THE GRADUATE SCHOOL OF NATURAL AND APPLIED SCIENCES
OF
MIDDLE EAST TECHNICAL UNIVERSITY

BY

BURAK ÇAĞRI DURAN

IN PARTIAL FULFILLMENT OF THE REQUIREMENTS
FOR
THE DEGREE OF MASTER OF SCIENCE
IN
ENGINEERING SCIENCES

FEBRUARY 2020

Approval of the thesis:

EFFECT OF GIRDER SPACING ON THE CONSTRUCTION COST AND SEISMIC PERFORMANCE OF SLAB-ON-PRESTRESSED CONCRETE GIRDER HIGHWAY BRIDGES

submitted by **BURAK ÇAĞRI DURAN** in partial fulfillment of the requirements for the degree of **Master of Science in Engineering Sciences, Middle East Technical University** by,

Prof. Dr. Halil Kalıpçılar
Dean, Graduate School of **Natural and Applied Sciences** _____

Prof. Dr. Murat Dicleli
Head of the Department, **Engineering Sciences** _____

Prof. Dr. Murat Dicleli
Supervisor, **Engineering Sciences, METU** _____

Examining Committee Members:

Assoc. Prof. Dr. Ferhat Akgül
Engineering Sciences, METU _____

Prof. Dr. Murat Dicleli
Engineering Sciences, METU _____

Prof. Dr. Tolga Akış
Civil Engineering, Atılım University _____

Date: 18.02.2020

I hereby declare that all information in this document has been obtained and presented in accordance with academic rules and ethical conduct. I also declare that, as required by these rules and conduct, I have fully cited and referenced all material and results that are not original to this work.

Name, Last name : Burak Çağrı Duran

Signature :

ABSTRACT

EFFECT OF GIRDER SPACING ON THE CONSTRUCTION COST AND SEISMIC PERFORMANCE OF SLAB-ON-PRESTRESSED CONCRETE GIRDER HIGHWAY BRIDGES

Duran, Burak Çağrı
Master of Science, Engineering Sciences
Supervisor : Prof. Dr. Murat Dicleli

February 2020, 56 pages

This study examines the effect of using different girder spacing on the total bridge construction cost in varied seismic zones. For this purpose, a number of structural models are built utilizing the finite element analysis to study the superstructure and substructure of a benchmark bridge in detail. Using these models, related parametric analyses are conducted for altering girder spacing, span lengths, number of spans, column heights, soil types and seismic zones. Ninety-five bridges with distinct types of superstructures and substructures are then designed and analyzed. Finally, pertinent construction costs are estimated for each bridge model under consideration. Comparison of costs revealed that an increase in girder spacing leads to a decrease in the total bridge construction cost. Moreover, seismic performance analyses of the bridges showed that no considerable change in terms of seismic performance observed with the increase in the girder spacing.

Keywords: Prestressed Concrete Girders, Bridge Design, Non-linear modeling, Cost Estimation, Seismic Performance

ÖZ

KİRİŞ ARALIĞININ ÖNGERİLMELİ BETON KİRİŞ ÜZERİNE TABLİYELİ KARAYOLU KÖPRÜLERİNİN YAPIM MALİYETİNE VE DEPREM PERFORMANSINA ETKİSİ

Duran, Burak Çağrı
Yüksek Lisans, Mühendislik Bilimleri
Tez Yöneticisi: Prof. Dr. Murat Dicleli

Şubat 2020, 56 sayfa

Bu çalışmada farklı deprem bölgelerinde bulunan köprülerde, öngermeli kirişler arasındaki mesafelerin, inşaat maliyetleri üzerindeki etkisi incelenmiştir. Bu amaçla, örnek bir köprü düşünülmüş ve bu örnek köprüye ait detaylı alt yapı ve üst yapı modelleri sonlu elemanlar yöntemi kullanılarak oluşturulmuştur. Oluşturulan bu modeler kullanılarak, farklı öngermeli kirişler arası mesafe, köprü açıklığı, açıklık sayısı, zemin sınıfı ve deprem bölgeleri için parametrik çalışma yapılmıştır. Birbirinden farklı toplam 95 adet köprüye ait analizler tamamlanmış ve köprüler tasarlanmıştır. Sonuç olarak bu köprülere ait inşaat maliyetleri elde edilmiştir. Maliyetlerin karşılaştırması sonucu, öngermeli kirişler arası mesafenin artmasının toplam köprü inşaat maliyetlerinde düşüşe sebep olduğu ortaya çıkmıştır. Ayrıca, köprülerin deprem performansı analizleri sonucunda, performans açısından önemli bir değişiklik gözlemlenmemiştir.

Anahtar Kelimeler: Öngerilmeli Beton Kirişler, Köprü Tasarımı, Doğrusal Olmayan Modelleme, Maliyet Tahmini, Deprem Performansı

To my father.

ACKNOWLEDGMENTS

First and foremost, I am deeply grateful for the continuous support, insight and patience of my supervisor, Prof. Dr. Murat Dicleli. Without his constant trust and guidance, I would not be able to complete this thesis. I have learnt so much from him and he was always there to steer me in the right direction, whenever I needed.

Besides my advisor, I would like to thank to my friend and colleague, Çağrı Demir for their encouragement and insightful comments.

Also, I would like to thank to my family, my father İbrahim Duran, my mother Necla Duran and my brother Barış Çağlar Duran. They have always believed in me and supported me every way they could. I dedicated this thesis to them.

TABLE OF CONTENTS

LIST OF TABLES

TABLES

LIST OF FIGURES

FIGURES

CHAPTER 1

INTRODUCTION

Turkey is an AASHTO affiliate state and therefore, bridges in Turkey are designed using AASHTO LRFD Bridge Design Specifications, 8th Edition (2017) (AASHTO – LRFD). This excludes the use of standard AASHTO girder types. Typical cross-sections of bridge girders widely employed in Turkey are T90, T120, T150, T180, T200. The details of these girder types will be given in the subsequent sections.

Prestressed concrete girders are widely used for highway bridges in Turkey, and these girders are usually placed side by side with a minimum gap of 20-25 mm between adjacent girders to accommodate construction tolerances. Such a construction method is preferred by the Turkish General Directorate of Highways since it allows the bridge decks to be constructed with minimal formwork and produces a speedy construction of the bridge superstructure. Such a construction practice, however, requires an excessive use of girders and hence, an increased mass of the superstructure. The increased mass of the superstructure in turn may cause amplified seismic design forces which may result in larger substructure components. Therefore, it is anticipated that the larger number of girders combined with larger substructure components may result in a higher construction cost of the bridge.

Various researchers investigated the problem of bridge cost optimization. For instance, Lounis and Cohn (1993) thoroughly explored the slab-on-prestressed-concrete-girder bridge superstructure parameters such as girder type, girder spacing, slab thickness, in order to achieve an optimal superstructure design for various span lengths and bridge widths. Sirca and Adeli (2005) also performed superstructure cost optimization of slab-on-prestressed-concrete-girder bridges with respect to similar parameters using neural networks algorithms. Batikha, Al Ani and Elhag (2017) investigated the effect of different girder types with various span lengths on the bridge superstructure construction and future maintenance costs. A study by

Adibaskoro and Suarjana (2019) utilized genetic algorithm approach for the optimization of prestressed concrete I–girder cross section geometry, while girder spacing and other relevant bridge parameters were kept constant. Similarly, Rabbat et. al (1984) proposed modified AASHTO standard precast concrete girder sections for cost-optimized design. Rana et al. (2013) implemented Evolutionary Operation (EVOP) algorithm to achieve cost minimization of two-span, continuous, prestressed concrete girders considering several girder and slab parameters. A study conducted by Ahsan et al. (2012) investigated the cost optimization of bridges having post-tensioned I girders. Yu et al. (1986) studied the cost-optimization of prestressed concrete box girders. A study by Aydın and Ayvaz, (2013) used genetic algorithm to determine the most cost-efficient span and subsequent superstructure cross section. The piers and footings were not optimized but were included in the cost estimation for a certain valley shape determining the heights of the piers.

Nevertheless, the majority of the above-mentioned research studies are concentrated solely on the optimization of the superstructure cost. Only the study performed by Aydın and Ayvaz, (2013) considered the overall cost optimization of the bridge but the seismic forces were neglected. Therefore, especially for the Turkish market, a research study is urgently needed to assess the cost efficiency of using side by side girders compared to widely spaced girders for bridges built in various seismic zones. Even if it has a lower construction cost, a bridge with poor seismic performance may have a high risk of collapse resulting in a total economic loss in areas with high risk of seismic activity. Therefore, regardless of the construction cost of bridges, their seismic performance as a function of the girder spacing is also worthy of investigation in regions with high risk of seismic activity such as Turkey, US or Japan.

1.1 Objective, Scope and Assumptions

The main objective of this research study is to assess the overall construction cost and seismic performance of slab-on-prestressed-concrete-girder bridges designed

and built by following the current state of design practice in Turkey where the superstructure is built by placing the girders side-by-side with a gap of 20-25 mm between the top flanges to avoid the use of formwork for casting the slab, in relation to cases where the girder are widely spaced.

The scope of this research study is limited to slab-on-prestressed-concrete-girder single and multiple-span, symmetrical, non-skew bridges typically used in Turkey. In these bridges the girders of each span are simply supported, but the slab is continuous along the length of the bridge per current state of design and construction practice in Turkey. The bridges are assumed to have single, two, three and four spans with span lengths varying between 20 and 40 meters. The width of the bridges is assumed to be 12 meters. The abutments are assumed to be seat type with a total height of six meters. The piers are assumed to be composed of a cap beam supported by two circular columns. Both the abutments and piers are assumed to rest on spread footings.

1.2 Research Outline

The outline of the research study is listed below:

i. As mentioned earlier, the slab-on-prestressed-concrete-girder bridges in Turkey are designed and built by placing the girders side-by-side with a gap of 20-25 mm between the top flanges to avoid the use of formwork for casting the slab. This type of a girder spacing is called the minimum girder spacing (S_{min}) within the context of this research study. To assess the construction cost and seismic performance of bridges designed according to the current state of design practice in Turkey in relation to bridges designed per conventional design approach where the girders are widely spaced, the girder spacing is kept as a variable. Accordingly, the girder spacing is assumed to be S_{min}, 1.5, 2.0, 2.5 and 3.0 meters. In addition to girder spacing, the span length, number of spans, column height, soil type and seismic zone are also varied to arrive to a general conclusion regarding the construction cost and

seismic performance efficiency of the superstructure design practice in Turkey compared to conventional design practice where the girder spacing is much larger.

ii. Next, the prestressed concrete girders of bridges considered in this research study are designed for each girder spacing and span lengths of 20, 25, 30, 35 and, 40 meters, under the H30-S24 AASHTO truck loading, which is recommended for the design of bridges in Turkey. The girder type, the number of girders, the number and arrangement of the prestressing tendons as well as the regular reinforcement of the girders are determined in this step.

iii. Subsequently, the substructures of 95 different bridges with varying girder spacing, span lengths and associated girder types, number of spans, column heights, soil types and seismic zones are designed in compliance with AASHTO (2017).

iv. Next the bill of quantities and associated construction cost of each bridge is calculated using the most up-to-date construction unit prices released yearly by the General Directorate of Highways in Turkey. The calculated construction costs are compared, and it is shown that as the girder spacing increase, the construction costs are notably reduced.

v. Finally, the nonlinear structural models of the bridges considered in this research study are built using the structural analysis software SAP2000. In the structural model the nonlinearity of the structural members, the possible impact between the superstructure and abutment back-wall as well as soil-structure interaction at the abutments and foundations are considered. Next, nonlinear time history analyses (NTHA) of the bridges are performed. The analyses results are presented as a function of girder spacing for various bridge parameters such as the number of spans, span length, column height and peak ground acceleration.

CHAPTER 2

DEFINITION OF THE BENCHMARK BRIDGE AND PARAMETERS CONSIDERED IN THE ANALYSES

2.1 Properties of the Benchmark Bridge

A two-span symmetrical slab-on-girder benchmark bridge, with spans of 30 m reflecting the design practice in Turkey, is selected. The bridge superstructure is composed of T120 type of girders spaced at 1.30 m and a 0.25 m thick reinforced concrete slab. The properties of the T-type prestressed concrete girders commonly used in Turkey are given in Figure 2.1., Table 2.1 and Table 2.2. A deck width of 12 meters accommodating 9 T120 girders is selected for the benchmark bridge since it allows for two vehicular design lanes. The selected deck width also allows for a minimum number of four girders to be placed in the superstructure when the girder spacing is selected as three meters in parametric studies, since less than four girders in bridge superstructures is uncommon for highway bridges. The height of the pier and seat type abutments are 12.5 m (column height is 11 m) and 6 m respectively. The pier is composed of two circular columns with a diameter of 1.3 m and a 2.0 x 1.5 m (Width x Height) rectangular cap beam. A 12.0 x 4.0 x 1.5 m (Length x Width x Thickness) rectangular spread footing is used to support the piers. The schematic drawings of the benchmark bridge are given in Figure 2.2 and Figure 2.3.

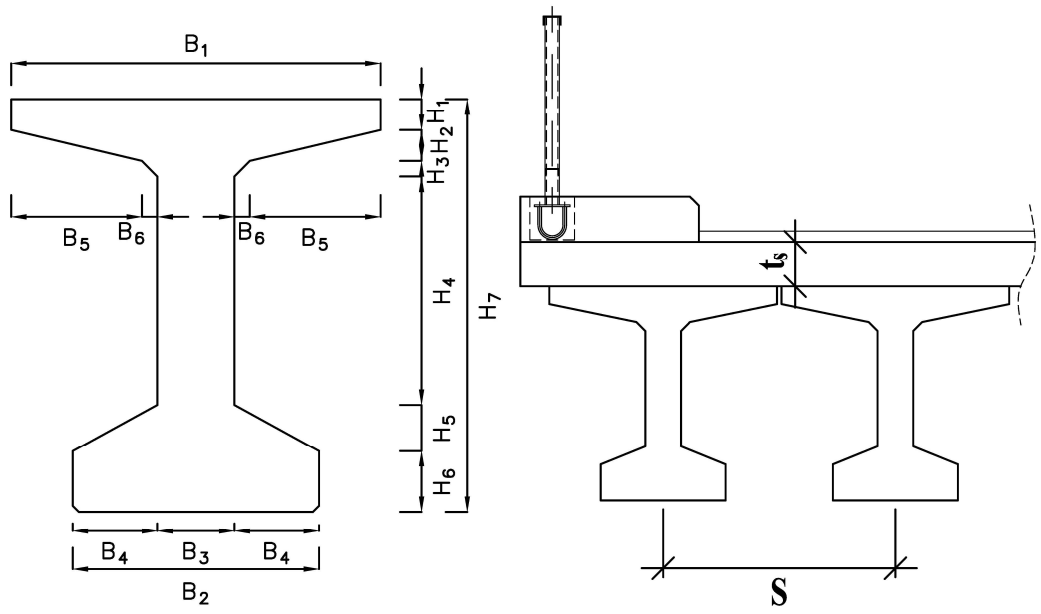

(a) (b)

Figure 2.1. (a) Girder parametric dimensions (b) Girder spacing (*S*) and slab thickness (t_s)

Table 2.1 Sectional properties of the prestressed concrete girders

Girder Type	A (m^2)	I_x (m^4)	I_y (m^4)	Weight per meter (kN/m)
T90	0.290	0.0302	0.00723	7.250
T120	0.534	0.102	0.0301	13.344
T150	0.608	0.181	0.0280	15.188
T180	0.779	0.320	0.0340	19.469
T200	0.829	0.419	0.0343	20.719

Table 2.2 Dimensions of the girder types in millimeters (See Figure 2.1.(a))

	Girder Type				
	T90	T120	T150	T180	T200
B_1	800	1275	1200	1200	1200
B_2	500	700	700	800	800
B_3	150	200	200	250	250
B_4	175	250	250	275	275
B_5	325	487.5	450	425	425
B_6	0	50	50	50	50
H_1	100	100	100	100	100
H_2	75	100	100	100	100
H_3	0	50	50	50	50
H_4	500	650	900	1150	1350
H_5	75	100	100	150	150
H_6	150	200	250	250	250
H_7	900	1200	1500	1800	2000

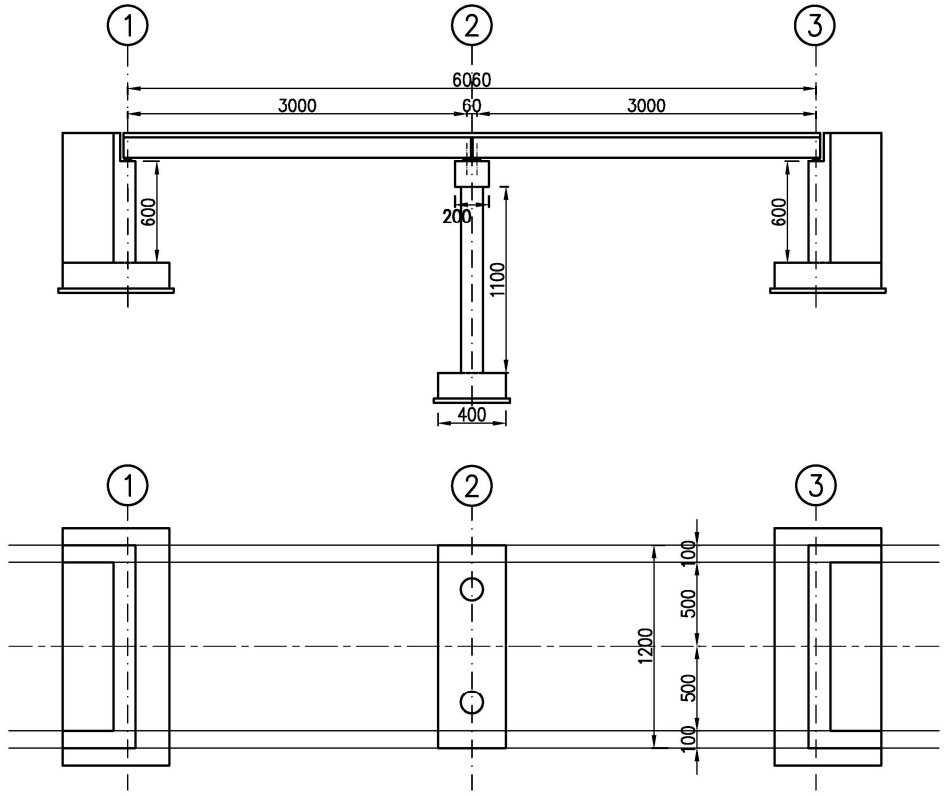

Figure 2.2. Elevation (top) and plan (bottom) view of the benchmark bridge (Dimensions are in centimeters, drawings are not in scale.)

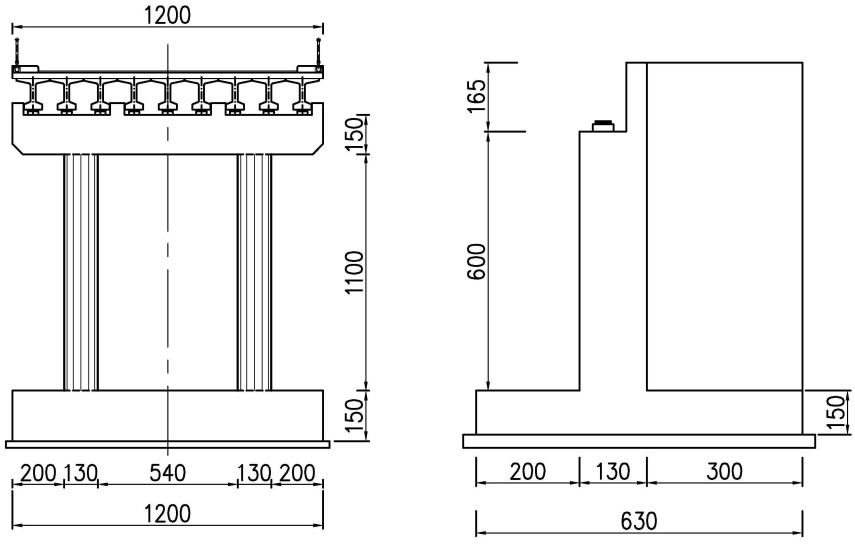

Figure 2.3. Typical cross-sections of (a) pier, (b) abutment of the benchmark bridge (Dimensions are in centimeters, drawings are not in scale.)

2.2 Parameters Considered in the Analyses

The benchmark bridge, which is presented in the above section, is modified and redesigned for the parametric studies. The design of the bridge is repeated each time a new value is assigned to the bridge parameter under consideration. These parameters and their range of values are given in Table 2.3. Based on these parameters, five analyses sets are considered and presented in the same table. In the table, the dominant parameter in each analysis set is shown in bold letters where the number of spans, span length, column height, soil type, and peak ground acceleration (PGA) are assigned a range of values. However, the girder spacing is altered in every analysis set, since it is the main parameter considered in this research study. In all the analysis cases, the bridge width is kept constant. A total of 95 bridges are considered in the analysis sets. It is noteworthy that, the dimensions of the bridge components given in Figures 2.2. and 2.3. are obtained from the analysis and design of the benchmark bridge. For all the other cases, each bridge is analyzed and designed where the girder type, column diameter, cap beam dimensions, foundation dimensions, and associated reinforcements are determined.

Table 2.3 Analyses sets

Analysis Set	Girder Spacing (m)	Number of Spans	Span Length (m)	Column Height (m)	PGA (g)	Soil Type
1	S_{min}, 1.5, 2, 2.5, 3	**1, 2, 3, 4**	30	11	0.4	C
2	S_{min}, 1.5, 2, 2.5, 3	2	**20, 25, 30, 35, 40**	11	0.4	C
3	S_{min}, 1.5, 2, 2.5, 3	2	30	**5.5, 11, 22**	0.4	C
4	S_{min}, 1.5, 2, 2.5, 3	2	30	11	**0.2, 0.4, 0.6, 0.8**	C
5	S_{min}, 1.5, 2, 2.5, 3	2	30	11	0.4	**B, C, D**

CHAPTER 3

DESIGN OF THE BRIDGES CONSIDERED IN THIS RESEARCH STUDY

3.1 Material Properties

For the bridges under consideration, the footings, piers, abutments and slab are assumed to be constructed using a concrete with 30 MPa characteristic strength and a modulus of elasticity of 26291MPa. The prestressed concrete girders are assumed to have a concrete strength of 45 MPa and a modulus of elastic of 32199 MPa. The steel reinforcement has a yield strength of 420 MPa and modulus of elasticity of 200000 MPa. The prestressing steel used in the girders is a low relaxation seven wire tendon with a diameter of 15.24 mm, yield and tensile strengths of 1674 and 1860 MPA respectively and modulus of elasticity of 197000 MPa.

3.2 Load Considered in the Analyses

Dead loads are composed of self-weights of the bridge components and weights of asphalt pavement and railings.

Live load in this study is composed of H30-S24 design truck (Figure 3.1.) and a lane load of 9.3 kN/m. A dynamic allowance is also included in the live load effects. Appropriate live load distribution factors in the AASHTO-LRFD are used for designing the bridge girders.

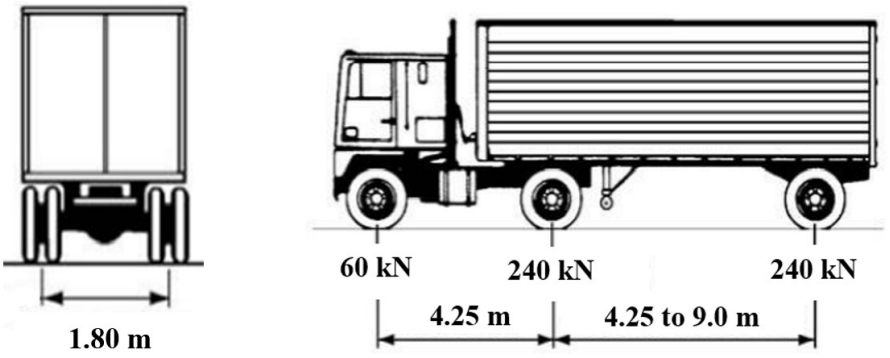

Figure 3.1. H30-S24 Truck

Lateral earth loads are calculated using Rankine's active earth pressure formula. However, Mononobe-Okabe method is used for lateral earth loads under seismic effects as described in AASHTO LRFD Appendix 11.

The seismic analyses are performed using the response spectrum method. The response spectra used in the analyses are constructed following the guidelines of Turkish Disaster and Emergency Management Presidency. For the benchmark bridge, a peak ground acceleration (PGA) of 0.4g and site soil classification C are used. The response spectrum used in the seismic analyses of the benchmark bridge is given in Figure 3.2. However, in the case of parametric studies, as mentioned earlier, both the PGA and soil type are modified.

For the design of the bridge pier columns under seismic forces, response modification factors of R = 5 and R = 3 are used for the transverse and longitudinal direction responses of the bridge respectively as given in Table 3.10.7.1-1 of the AASHTO – LRFD (2017) for a multiple-column pier system. Capacity design approach is used in the design of the cap beam and footing using the estimated plastic moment capacity of the pier columns.

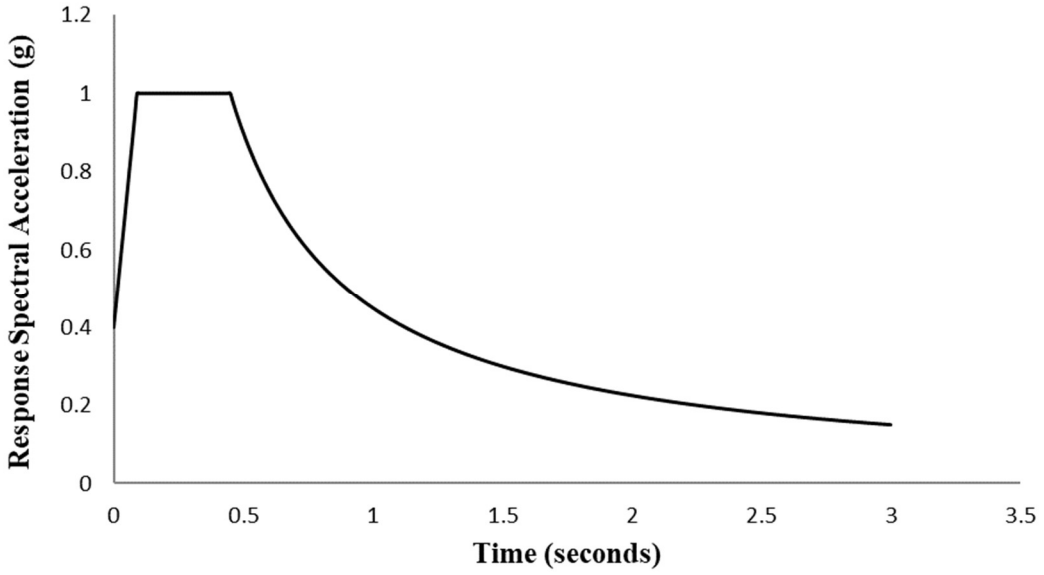

Figure 3.2. Response spectrum for 0.4 g PGA, C type soil

3.3 Design of the Bridge Superstructures

For the bridges considered in this study, the prestressed girder type (Table 3.1), the number of prestressing tendons and their placement as well as the cross-section area and placement of regular reinforcement are determined for each combination of span lengths and girder spacing. As mentioned earlier, according to the design practice in Turkey, prestressed concrete girders are usually simply supported. Therefore, no prestressing tendons are required in the top flanges. Accordingly, straight tendons are used in the bottom flange along the length of the girder. For the end regions of the simply supported girders where the design moments are decreased, up to 50% of the prestressing tendons are debonded gradually near the end region of the girders using plastic sheathing to prevent compression failure of the concrete in the top flange.

The bridge slab is designed as a continuous beam spanning over the girders under its self-weight, weight of the asphalt pavement and the heavy axles of the H30 – S24 truck per current state of design practice in Turkey.

Table 3.1 Prestressed concrete girder sections selected for each combination of span length versus girder spacing

L (m)	S_{min}	S=1.5 m	S=2 m	S=2.5 m	S=3 m
20	T90	T120	T120	T120	T120
25	T120	T120	T120	T150	T150
30	T120	T120	T150	T150	T180
35	T150	T150	T180	T180	T180
40	T180	T180	T180	T200	T200

3.4 Design of Bearings

The dimensions of the elastomeric bearings are determined following the provisions of the AASHTO-LRFD. Accordingly, the total height of the elastomeric bearings are determined such that the lateral displacement of the bearings under seismic loadings

is smaller than 50% of their height. The plan dimensions of the elastomeric bearings are selected to fulfill the AASHTO-LRFD requirements under loadings other than seismic loads.

3.5 Design of the Bridge Substructures

3.5.1 Seismic Model Used in the Analyses

The seismic models of the bridges considered in this research study are built using the structural analysis program SAP2000 using 3-D frame elements and links as shown in Figure 3.3. The superstructure of the bridges is idealized as a single 3-D frame element representing the composite section of the girders and the slab. The piers are modeled using 3-D frame elements. The cap-beam-column joints are modeled using rigid frame elements. The ends of the superstructure and substructure frame elements are connected to fictive rigid beam elements at the pier and abutment bearing locations to accurately simulate the position of the superstructure centroid with respect to the cap beam centroid and bearings. The bearings are idealized using cantilever frame elements with circular cross-sections. The height of the frame element representing the elastomeric bearing is set equal to the total height of the elastomeric bearing and the flexural stiffness, *EI* of the frame element is then, calculated by setting the stiffness of the frame element equal to that of the bearing as follows:

$$EI = \frac{G\ x\ A\ x\ h_{rt}^2}{3} \quad (1)$$

G is the shear modulus of the elastomeric bearing and it is equal to 1.0 MPa at 20°C, *A* is the plan area of the bearing, and h_{rt} is the total rubber height.

The frame elements representing the elastomeric bearings are then connected between the bottom of the superstructure and top of the substructure (bearing pedestal). A moment release is introduced at the top of the frame elements representing the bearings.

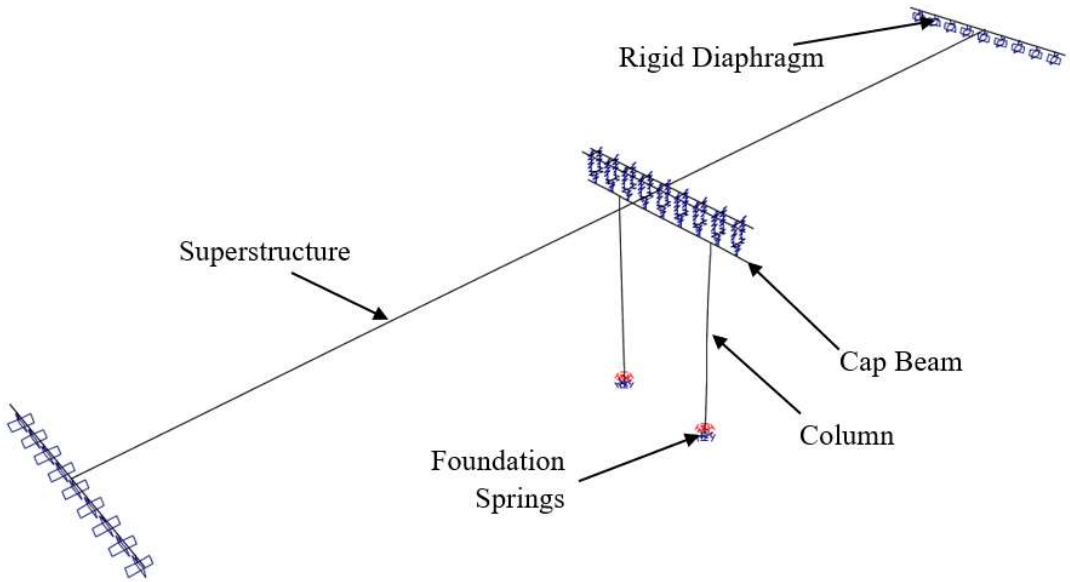

(a)

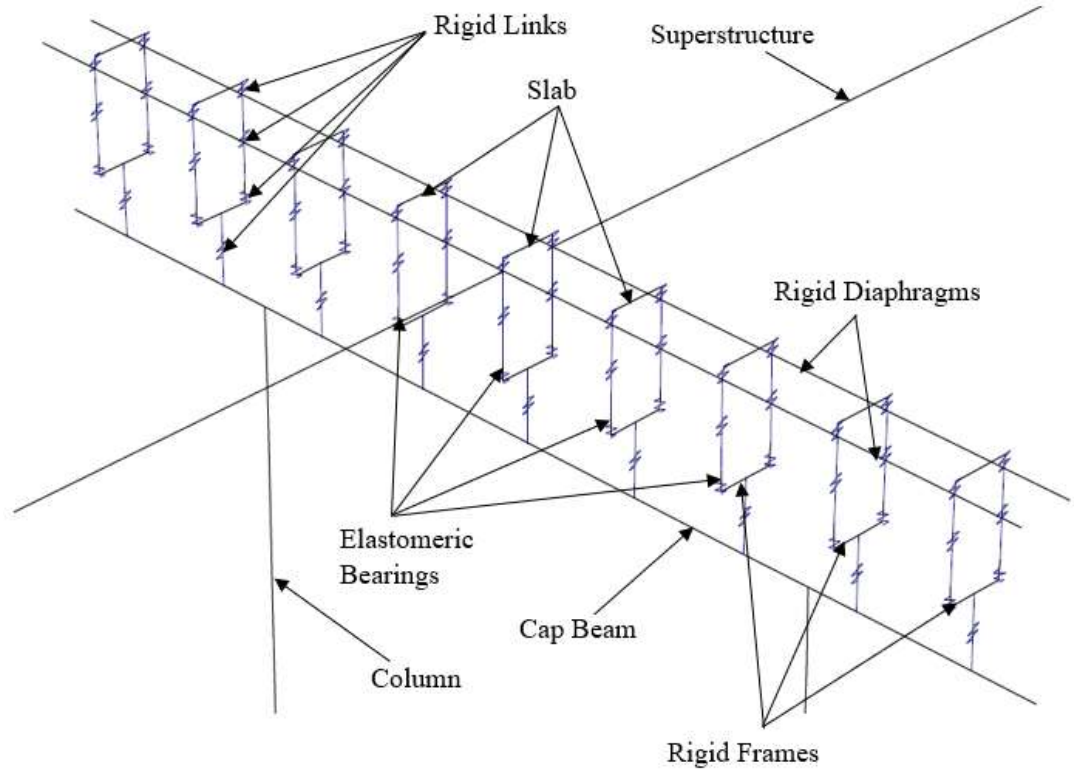

(b)

Figure 3.3. Seismic model, (a) overall view, (b) detail view of the pier

According to the design practice in Turkey, the bridge is allowed to move in the longitudinal direction to accommodate movements due to creep, shrinkage and thermal fluctuations but restrained in the transverse direction to resist wind forces. This design practice is reflected into the model for seismic analyses. The transverse direction fixity condition of the bridge is achieved by assigning a large lateral translational stiffness for the elastomeric bearings in the structural model.

The soil-structure interaction at the rectangular spread footings supporting the piers are idealized using three translational and three rotational uncoupled boundary springs connected at the interface nodes of soil and rectangular spread footings (Figure 3.4.). The method proposed by Dorby and Gazetas (1986) including the effect of the embedment depth of the footing is employed in the calculation of the stiffness of the boundary springs for the vertical, horizontal (K_x and K_y), rocking (K_z) and torsional modes (K_{xx}, K_{yy} and K_{zz}) as follows:

$$K_x = \frac{GB}{2-\nu}\left[3.4\left(\frac{L}{B}\right)^{0.65} + 1.2\right]\left(1 + 0.21\sqrt{\frac{D}{B}}\right)\left[1 + 1.6\left(\frac{hd(B+L)}{BL^2}\right)^{0.4}\right] \quad (2)$$

$$K_y = \frac{GB}{2-\nu}\left[3.4\left(\frac{L}{B}\right)^{0.65} + 0.4\frac{L}{B} + 0.8\right]\left(1 + 0.21\sqrt{\frac{D}{B}}\right)\left[1 + 1.6\left(\frac{hd(B+L)}{BL^2}\right)^{0.4}\right] \quad (3)$$

$$K_z = \frac{GB}{1-\nu}\left[1.55\left(\frac{L}{B}\right)^{0.75} + 0.8\right]\left[1 + \frac{1}{21}\frac{D}{B}\left(2 + 2.6\frac{B}{L}\right)\right]\left[1 + 0.32\left(\frac{d(B+L)}{BL}\right)^{2/3}\right] \quad (4)$$

$$K_{xx} = \frac{GB^3}{1-\nu}\left[0.4\left(\frac{L}{B}\right) + 0.1\right]\left(1 + 2.5\frac{d}{B}\left[1 + \frac{2d}{B}\left(\frac{d}{D}\right)^{-0.2}\sqrt{\frac{B}{L}}\right]\right) \quad (5)$$

$$K_{yy} = \frac{GB^3}{1-\nu}\left[0.47\left(\frac{L}{B}\right)^{2.4} + 0.034\right]\left(1 + 1.4\left(\frac{d}{L}\right)^{0.6}\left[1.5 + 3.7\left(\frac{d}{L}\right)^{1.9}\left(\frac{d}{D}\right)^{-0.6}\right]\right) \quad (6)$$

$$K_{zz} = GB^3\left[0.53\left(\frac{L}{B}\right)^{2.45} + 0.51\right]\left(1 + 2.6\left(1 + \frac{B}{L}\right)\left(\frac{d}{B}\right)^{0.9}\right) \quad (7)$$

where G is the effective shear modulus of the foundation soil, v is the Poisson's ratio of the soil, B, L and d are the footing dimensions as shown in Figure 3.5., D and h are the parameters related to the footing depth as shown in Figure 3.5.

The effective shear modulus, G, in the above equations is calculated by employing the initial shear modulus, G_0, expressed as follows (Federal Emergency Management Agency (FEMA) 356 (2000)):

$$G_0 = \frac{\gamma v_s^2}{g} \tag{8}$$

where γ is the unit weight of the soil, v_s is the shear wave velocity and g is the gravity constant. As stated in Geotechnical Engineering Circular No. 3 published by Federal Highway Administration (FHWA) (Kavazanjian et al., 1997), to reflect the reduced shear modulus under cyclic loadings, a reduction factor is applied to the initial shear modulus G_0 to calculate the effective shear modulus, G, for various site classes and levels of peak ground accelerations. For this purpose, the factors given in Table 3.2 published by the FEMA (FEMA 356 (2000)) were used.

Table 3.2 Effective shear modulus ratio (G/G_0)

	Effective Peak Acceleration			
Site Class	0	0.1	0.4	0.8
B	1	1.00	0.95	0.90
C	1	0.95	0.75	0.60
D	1	0.90	0.50	0.10

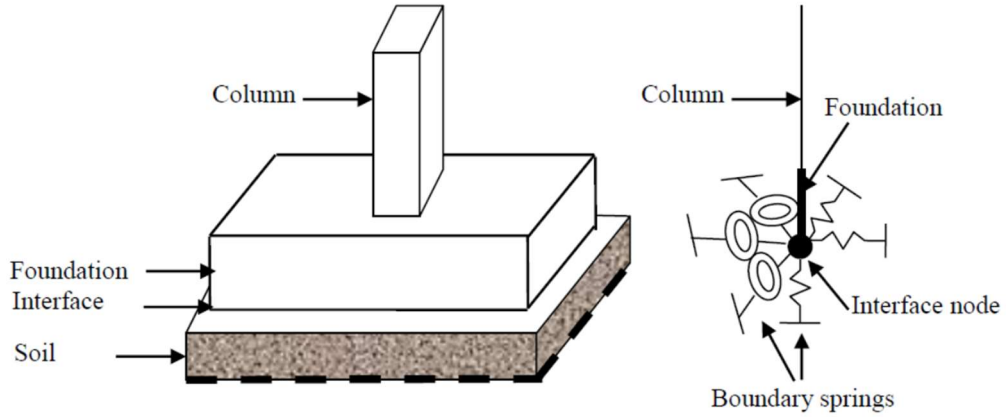

Figure 3.4. Soil-footing springs

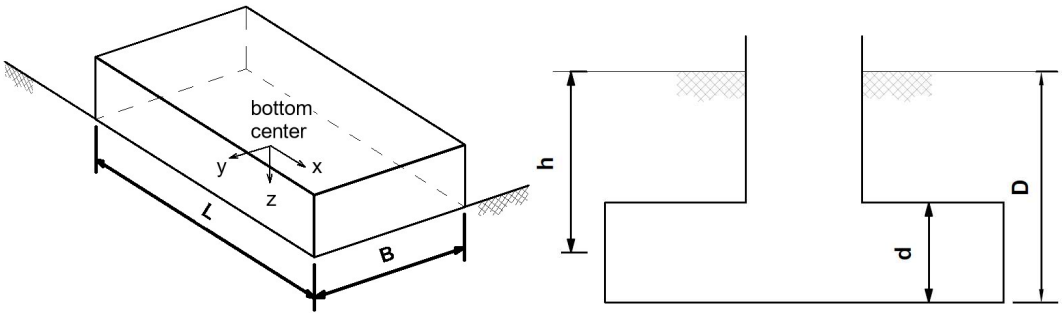

Figure 3.5. Foundation geometric parameters used in Equations 2-7. (L ≥ B).

3.5.2 Estimation of Cap Beam and Column Dimensions and Reinforcement for the Piers

The superstructure dead loads and vehicular loads are applied at the bearing locations on the cap beam and the internal forces in the cap beam and columns are determined for gravitational load analyses using a 3D frame model of the pier. The cap beam is assumed to be damage free under seismic loads per current state of design practice in Turkey. Accordingly, capacity design approach is followed for the design of the cap beam using the plastic moment capacities of the pier columns amplified by a

factor of 1.30. The shear reinforcement of the cap beam is then designed by following again the capacity design approach where the maximum seismic shear force in the cap beam is calculated by using the following equation:

$$V = \frac{2\,M_{pb}}{l_b} \tag{9}$$

where M_{pb} is the plastic moment capacity of the cap beam and l_b is the clear length of the cap beam between the two columns. Similarly, the shear reinforcement of the columns is designed by following the capacity design approach using the plastic moment capacity of the columns.

Slenderness requirements govern the column design for the case of 22-meter column, therefore larger cross-sectional column diameter is selected than the required by the sectional capacity calculations. However, in the case of 11-meter column, slenderness requirement is not the governing factor. Therefore, it was possible to design the pier using smaller diameter columns. The increased column diameter of the 22-meter column, hence, may lead to more rigid (less flexible) column.

3.5.3 Design of the Abutment and Footings

Intermediate footings and abutments are modelled with four – nodes, shell elements using the structural analysis program SAP2000. Elastic vertical springs are used at the bottom of the foundations, to model the stiffness of the soil for the SLS (Serviceability Limit State) analyses. For each soil type (B, C, D) in the AASHTO – LRFD, a representative stiffness value was considered for the vertical springs. The SLS (Serviceability Limit State) loads are applied on the model and the analyses are conducted to determine the internal forces and soil reactions for design purposes. No tension was observed in the springs in the analyses. In the case of the ULS (Ultimate Limit States) analyses, the soil reaction is assumed to be uniformly distributed as per AASHTO-LRFD (2017). First the intensity of the uniformly distributed soil pressure and its area of application are determined. Then, the model is modified by removing the springs (only four weak springs are used at the corners of the footing)

and the analyses are conducted by applying the uniform soil pressure as a load together with the ULS loads to determine the internal forces. The ULS reinforcements are determined based on the obtained internal forces.

CHAPTER 4

ANALYSIS RESULTS FOR DESIGN

4.1 Modal Vibration Periods versus Girder Spacing

Figures 4.1, 4.2 and 4.3 show the variation of the modal vibration periods as a function of girder spacing for various number of spans, column heights and span lengths, respectively. In the figures, it is observed that, for all the cases of number of spans, column heights and span lengths; modal vibration periods in both principal directions increase with the increase in the girder spacing. In an undamped single degree of freedom system (SDOF), the fundamental vibration period is expressed as follows:

$$T = 2\pi\sqrt{\frac{m}{k}} \tag{10}$$

where m is the mass and k is the stiffness of the SDOF. The same relationship may roughly apply to the dynamics of the bridges under consideration. According to Eqn. 10, when the total weight of the superstructure increases, the modal vibration period of the bridge also increases. On the other hand, when the stiffness of the substructure and/or the elastomeric bearings increases, the modal vibration period of the bridge decreases. In the case of the bridges under consideration, the number of girders used in the superstructure and associated mass increase with decreasing girder spacing. However, for bridges with smaller girder spacing, more elastomeric bearings are required to support the increased number of girders leading to larger lateral stiffness of the bridge. The rate of increase in the lateral stiffness of the bridge due to the increased number of elastomeric bearings is larger than the rate of increase in the mass of the superstructure due to the increased number of girders. This phenomenon results in smaller periods of vibration for the cases of smaller girder spacing. This, in turn, produces larger spectral acceleration in the case bridges with smaller girder spacing. As expected, bridges with longer span lengths (more mass) and taller piers (smaller lateral stiffness) have longer vibration periods (Figs. 4.2 and 4.3). In the case of the bridges with different number of spans, as the pier column sizes vary, a

certain trend is not observed for the period of vibration as a function of the number of spans.

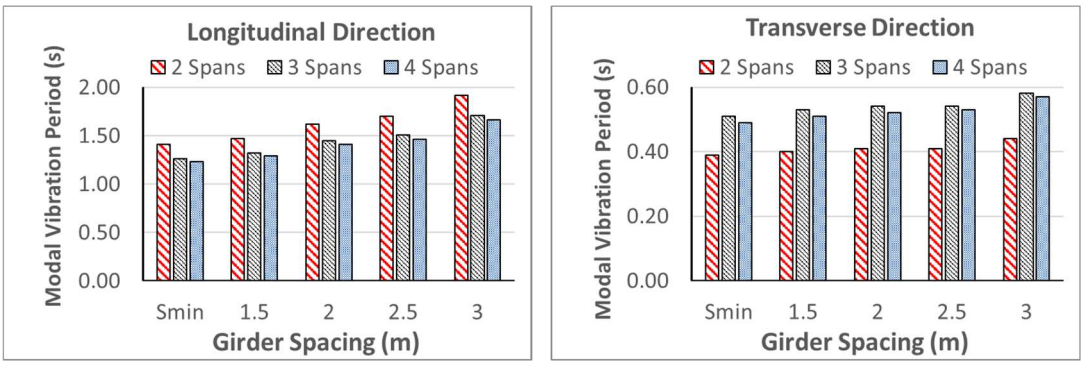

(a) (b)

Figure 4.1. Modal vibration periods in (a) longitudinal direction and (b) transverse direction versus girder spacing for different number of spans (2, 3 and 4 spans)

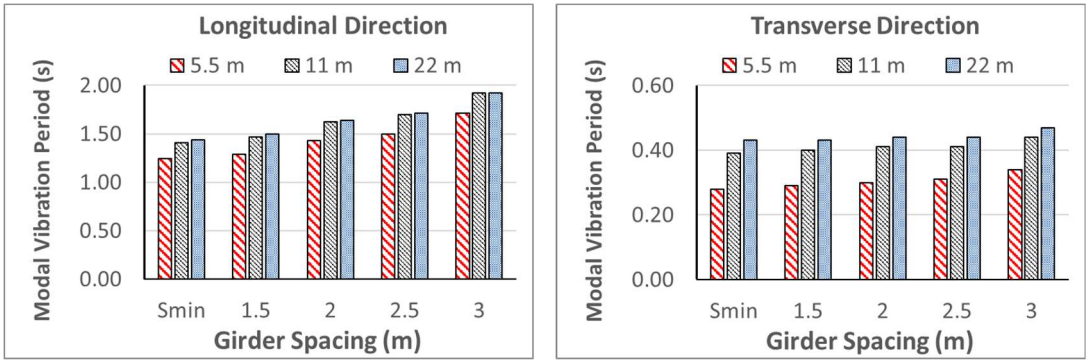

(a) (b)

Figure 4.2. Modal vibration periods in (a) longitudinal direction and (b) transverse direction versus girder spacing for different column heights (5.5 m, 11 m and 22 m)

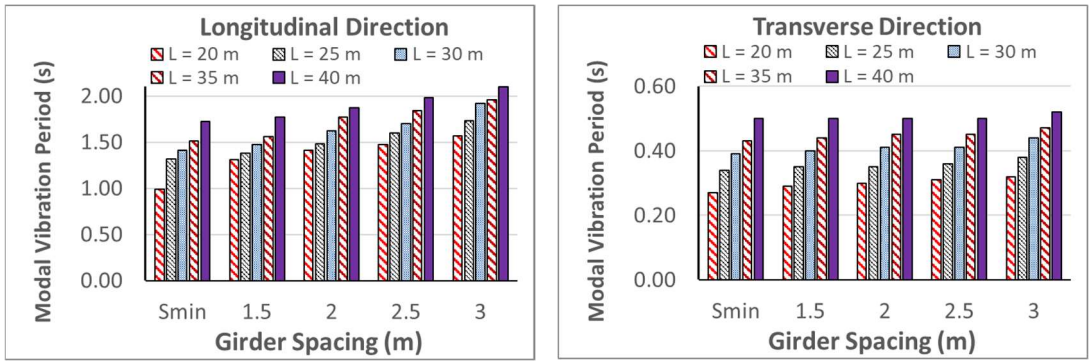

(a) (b)

Figure 4.3. Modal vibration periods in (a) longitudinal direction and (b) transverse direction versus girder spacing for different span lengths (20 m, 25 m, 30 m , 35m and 40 m)

4.2 Design Seismic Substructure Forces versus Girder Spacing

In this section, the effect of girder spacing on the magnitude of the design substructure forces is discussed as a function of various bridge structural parameters.

Figure 4.4. shows the maximum design pier forces as a function of the girder spacing for various number of spans. As observed from the figure, pier seismic forces decrease for larger girder spacing regardless of the number spans. It is also observed that the pier design seismic forces increase for larger number of spans. In the case of the bridges with larger number of spans, a smaller portion of the lateral seismic force is shared by the stronger abutments. This results in larger seismic forces in the piers. It is noteworthy that the design of the pier columns is governed by the transverse direction response of the bridge where larger column sizes for bridges with larger number of spans.

In Figure 4.5., seismic substructure forces versus girder spacing are presented for different column heights. The figure reveals that as the girder spacing increases, the seismic substructure forces decrease regardless of the column height. As expected, bridges with taller piers have larger column moments but lower shear forces. The fundamental vibration period of the bridge increases as the pier height increases due

to the reduction in the pier lateral stiffness. This results in smaller spectral accelerations (the period falls in the descending part of the design spectrum – Fig. 3.2.) and hence, smaller shear forces in the taller piers. However, the longer moment arm of the taller piers produce amplified design seismic moments.

In Figure 4.6., the variation of the pier seismic forces is presented as a function of girder spacing for various span lengths. As observed from the figure, pier seismic forces decrease as the girder spacing increases regardless of the span length. As expected, the pier seismic forces increase with increasing span lengths. This is mainly due to the larger tributary superstructure weight per pier for bridges with longer span lengths.

Figure 4.7. illustrates the change in the seismic substructure forces as a function of girder spacing for PGA values of 0.2 g, 0.4 g, 0.6 g and 0.8 g. As observed from the figure, pier seismic forces decrease as the girder spacing increases regardless of the PGA.

In Figure 4.8., seismic substructure forces versus girder spacing are shown in bar charts for different soil types. Figure 4.8. reveals that regardless of the soil type, the seismic substructure forces decrease with increasing girder spacing.

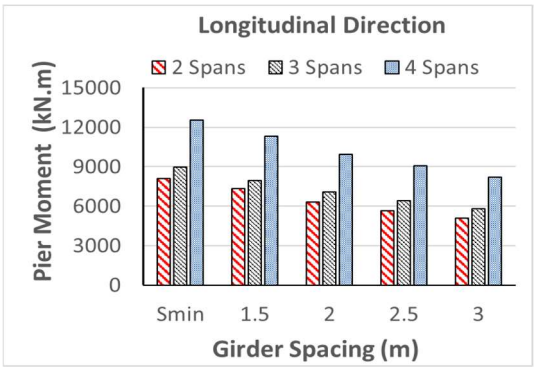

(a)

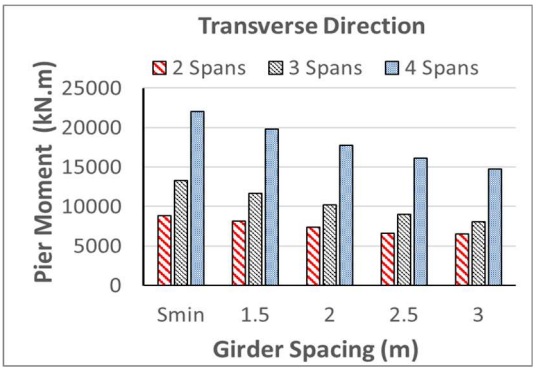

(b)

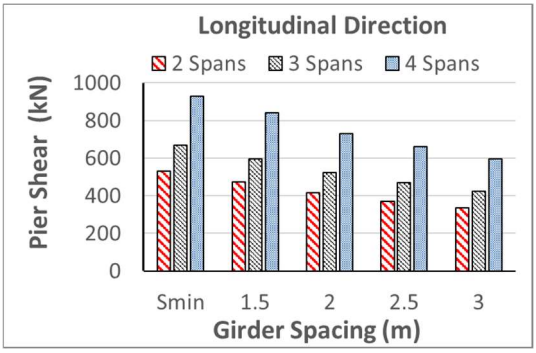

(c)

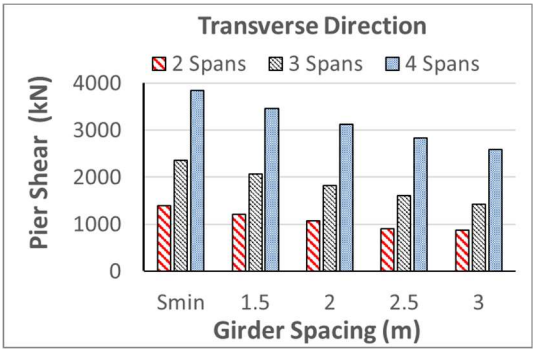

(d)

Figure 4.4. Pier moment in (a) longitudinal direction, (b) transverse direction; pier shear in (c) longitudinal direction, (d) transverse direction versus girder spacing for different number of spans (2, 3 and 4 spans)

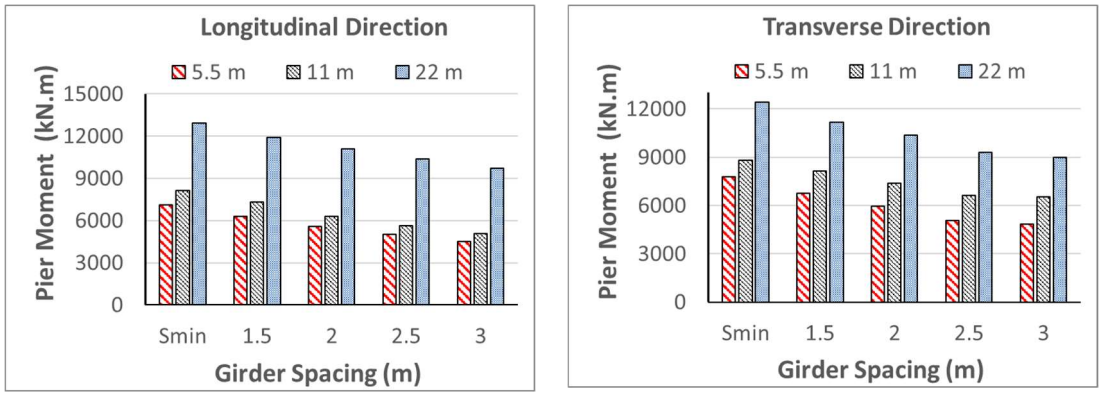

(a)

(b)

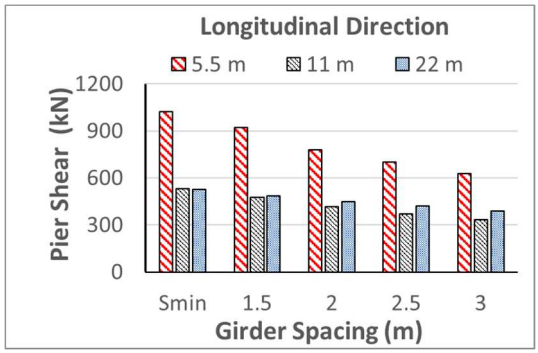

(c)

(d)

Figure 4.5. Pier moment in (a) longitudinal direction, (b) transverse direction; pier shear in (c) longitudinal direction (d) transverse direction versus girder spacing for various column heights (5.5 m, 11 m and 22 m)

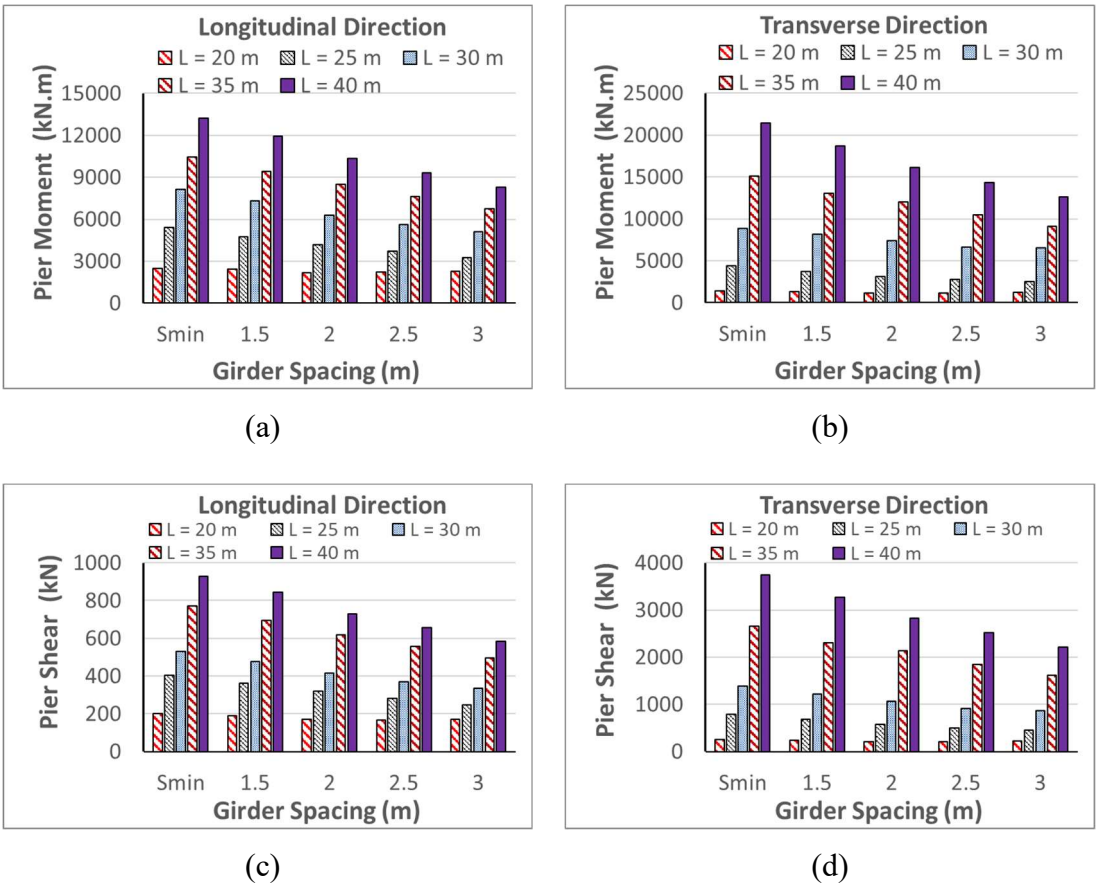

Figure 4.6. Pier moment in (a) longitudinal direction, (b) transverse direction; pier shear in (c) longitudinal direction, (d) transverse direction versus girder spacing for different span lengths (20 m, 25 m, 30 m , 35m and 40 m)

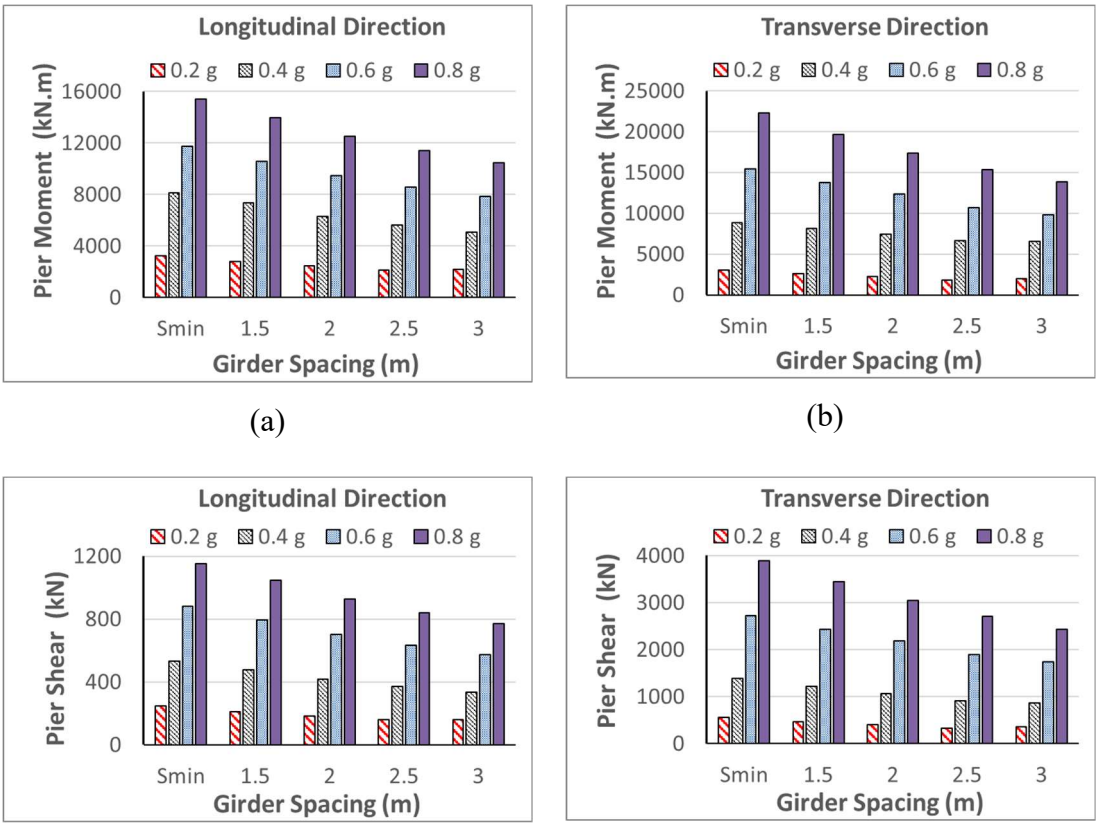

Figure 4.7. Pier moment in (a) longitudinal direction, (b) pier moment in transverse direction; pier shear in (c) longitudinal direction, (d) transverse direction versus girder spacing for different PGAs (0.2 g, 0.4 g, 0.6 g and 0.8 g)

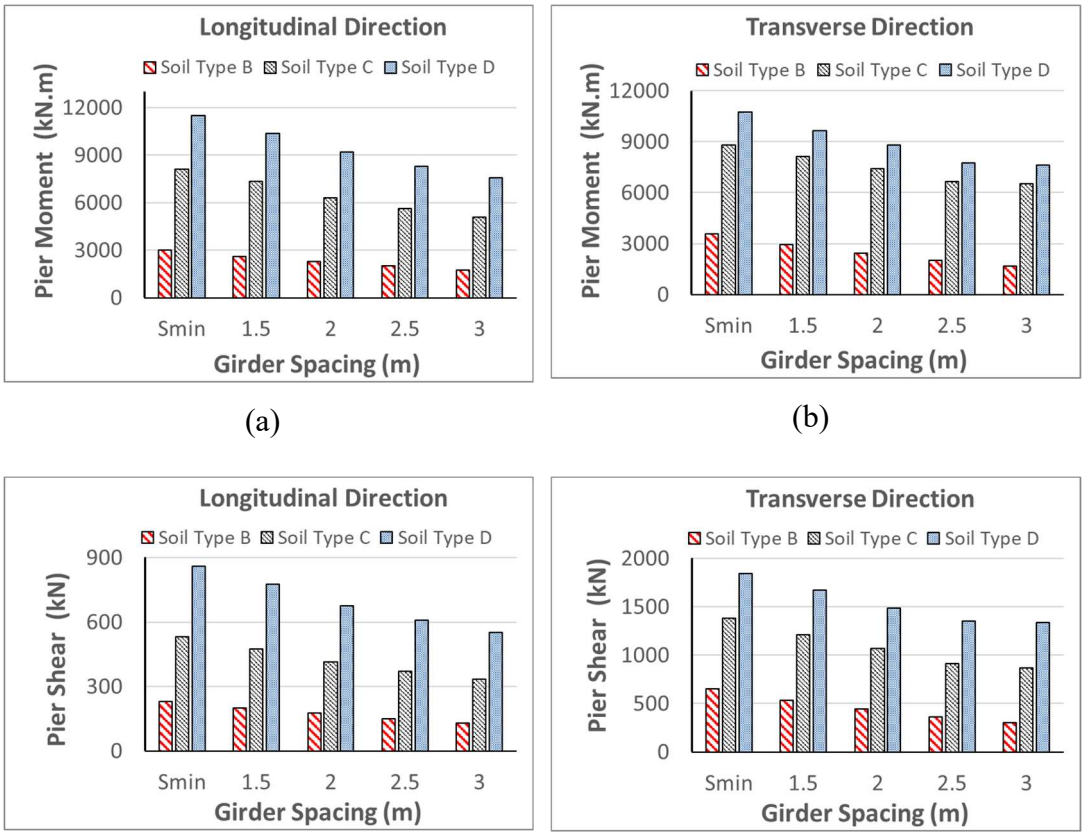

Figure 4.8. Pier moment in (a) longitudinal direction, (b) transverse direction; pier shear in (c) longitudinal direction, (d) transverse direction versus girder spacing for different soil types (Types B, C and D)

CHAPTER 5

COST ESTIMATION AND COMPARISON OF COSTS

5.1 Cost Estimation

Each bridge in the analysis sets presented in Table 3 is designed (in total 95 different bridges) in compliance with AASHTO LRFD Bridge Design Specifications (2017). Next, a bill of quantities for each bridge is obtained. The following table represents the items, which are included in the bill of quantities. Bill of quantities and estimation of construction costs for the benchmark bridge is presented in Table 5.2.

Table 5.1 Items included in the bill of quantities

Cost Item	Unit	Unit Cost (US Dollars)
Excavation for footings and abutments	m^3	10.07
Lean concrete under footings and abutment foundations	m^3	40.33
Concrete for structural components, except prestressed girders (formwork included)	m^3	89.06
Backfill of abutments	m^3	11.33
Scaffolding for cap beam construction	m^3	7.12
Concrete for prestressed girders	m^3	123.93
Lifting and placing of prestressed girders	tons	8.05
Reinforcing steel	tons	824.86
Prestressing tendons	tons	2912.29
Expansion joints	m	868.59
Elastomeric bearings	dm^3	10.74
Insulation of the deck	m^2	5.86
Railings	tons	1296.69

Table 5.2 Bill of quantities and total cost of the benchmark bridge

Cost Item	Unit	Quantity	Unit Price (USD)	Total Price (USD)
Excavation for footings and abutments	m^3	506.90	10.07	5,104.48
Lean concrete under footings and abutment foundations	m^3	63.36	40.33	2,555.41
Concrete for structural components, except prestressed girders (formwork included)	m^3	816.32	89.06	72,701.82
Lifting and placing of prestressed girders	tons	703.27	8.05	5,661.32
Concrete for prestressed girders	m^3	293.03	123.93	36,315.05
Backfill of abutments	m^3	459.00	11.33	5,200.47
Insulation of the deck	m^2	611.00	5.86	3,580.46
Scaffolding for cap beam construction	m^3	261.35	7.12	1,860.78
Reinforcing steel	tons	117.94	824.86	97,287.65
Expansion joints	m	24.00	868.59	20,846.16
Prestressing tendons	tons	16.32	2,912.29	47,528.93
Elastomeric bearings	dm^3	1,108.08	10.74	11,900.78
Railings	tons	5.94	1296.69	7,700.94
			Gross Total (USD)	318,244.25

The General Directorate of Highways in Turkey releases unit prices for construction works yearly. In this research study, the up-to-date unit prices as of 2019 are used in the calculation of the total construction costs of the bridges considered in this research study. However, the transportation costs are not included in the estimation of the construction costs.as the location of a bridge site with respect to the sources

of material supply may vary. Therefore, excluding the transportation cost produces a more rational comparison of the construction costs of the bridges considered in this research study. It is noteworthy that non-structural such as approach fills, asphalt pavement, road signs, lighting, etc. are not considered. Finally, the costs calculated are converted to US Dollars using the most up-to-date exchange rates.

Figure 5.1. presents the construction costs calculated as a function of girder spacing for each analysis case in a bar chart form. As observed from the figure, construction costs drop when the girder spacing increases regardless of the number spans, span length, column height, soil type and the level of PGA. The reduction in the bridge construction cost ranges between 11% and 22% when the girders are placed with a three-meter spacing, instead of using a minimum possible gap in-between. The difference between the construction costs becomes more notable as the number of spans increases.

As explained earlier, as the construction cost is proportional to the substructure forces and the effect of the variation in substructure forces as a function of different parameters was already discussed in earlier sections, no further discussion is needed. That is, longer span bridge with taller columns built on soft soil with minimum girder spacing have the maximum construction cost. Therefore, considering the cost, it is clear that the construction method in Turkey where the girders are placed side-by-side to avoid formwork costs is not a cost-effective method However, such an approach may have other merits regarding the seismic behavior of the bridge. This will be explored in the subsequent sections.

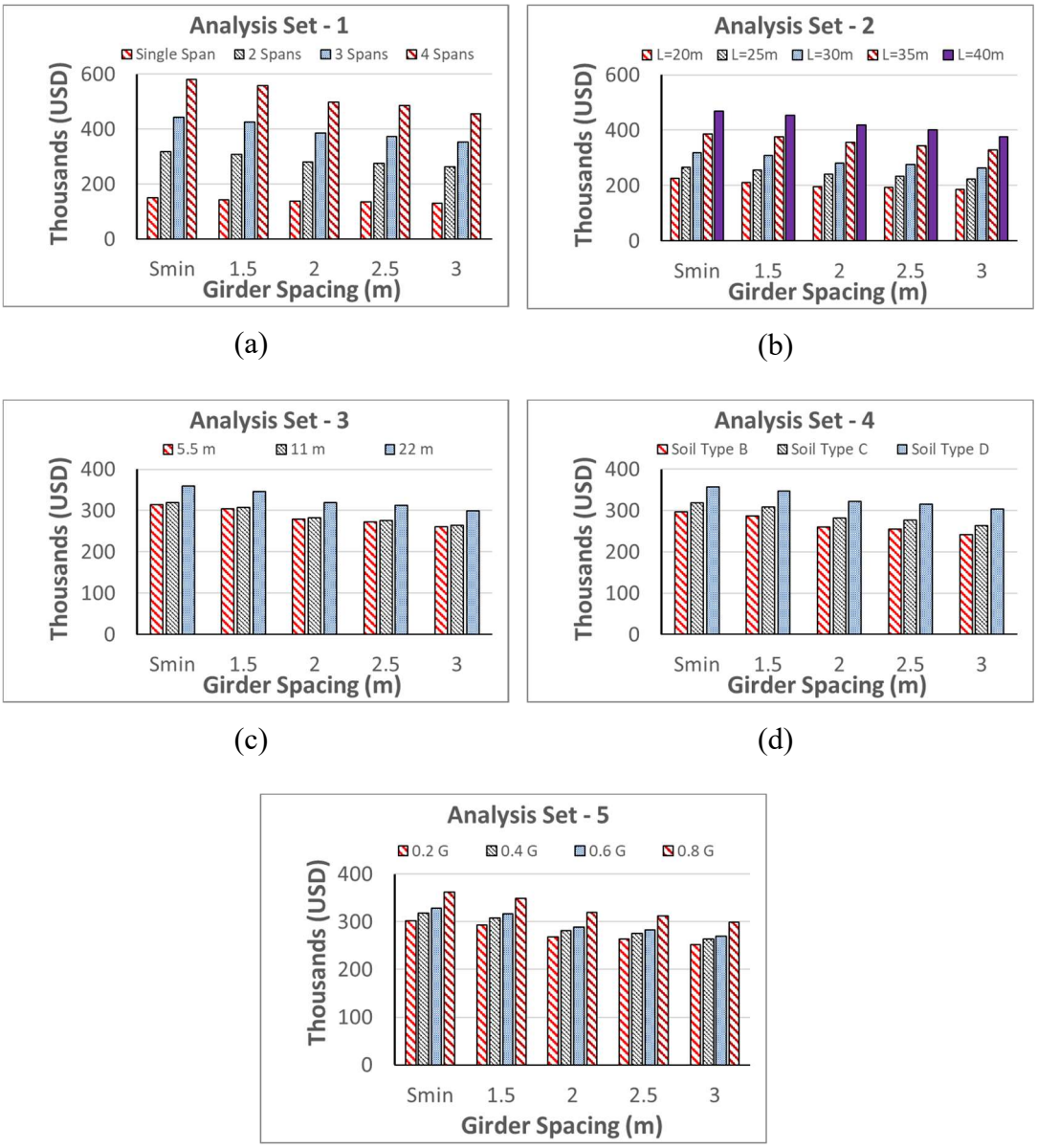

Figure 5.1. Comparison of construction costs

CHAPTER 6

SEISMIC PERFORMANCE ANALYSES

6.1 Bridge Parameters Considered in the Seismic Performance Analyses

To perform comparative seismic performance analyses for the bridges under consideration, the Analyses Sets presented in Table 6.1. are built. In the table, the main parameter is the girder spacing. The girders spacing assumes values of S = S_{min}, S = 2 m and S = 3 m. For each girder spacing, bridge parameters such as number of spans, span length, column height as well as the PGA representing the ground motion intensity are assigned a range of values to cover a broad range of possibilities while investigating the effect of the girder spacing on the seismic performance of bridges. This resulted in a total number of 30 analyses cases and 60 structural models for the longitudinal and transverse direction analyses of the bridges under consideration. Nonlinear time history analyses (NTHA) of the bridge structural models are performed and the analyses results are compared as a function of the girder spacing.

Table 6.1 Seismic Performance Analyses Sets

Analysis Set	Girder Spacing (m)	PGA (g)	Number of Spans	Span Length (m)	Column Height (m)	Soil Type
1	S_{min}, 2, 3	**0.2, 0.4, 0.6, 0.8**	2	30	11	C
2	S_{min}, 2, 3	0.4	**2, 3, 4**	30	11	C
3	S_{min}, 2, 3	0.4	2	**20, 30, 40**	11	C
4	S_{min}, 2, 3	0.4	2	30	**5.5, 11, 22**	C

6.2 Selected Ground Motions

For the NTHA, seven earthquake ground motions are selected such that the response spectra of the selected ground motions are compatible with the target design response spectrum, given in Figure 3.2, using the Pacific Earthquake Engineering Research (PEER) strong motion database. In Table 6.2., the details of the selected ground motions are given. The response spectra of the scaled ground motions and their average response spectra are given in Figure 6.1., along with the target design response spectra.

Table 6.2 Details of the Selected Ground Motions

Earthquake	Year	Magnitude	Station	Distance to Station (km)	A_p (g)
Loma Prieta	1989	6.93	Fremont - Mission San Jose	39.5	0.44
Chi-Chi_Taiwan	1999	7.62	TCU042	26.3	0.43
Chi-Chi_Taiwan06	1999	6.30	CHY024	31.1	0.51
Big Bear01	1992	6.46	Morongo Valley Fire Station	29.0	0.30
Iwate_Japan	2008	6.90	Kami_ Miyagi Miyazaki City	25.1	0.44
Niigata_Japan	2004	6.63	NIGH13	39.4	0.59
Chuetsu-oki_Japan	2007	6.8	Nadachiku Joetsu City	35.9	0.46

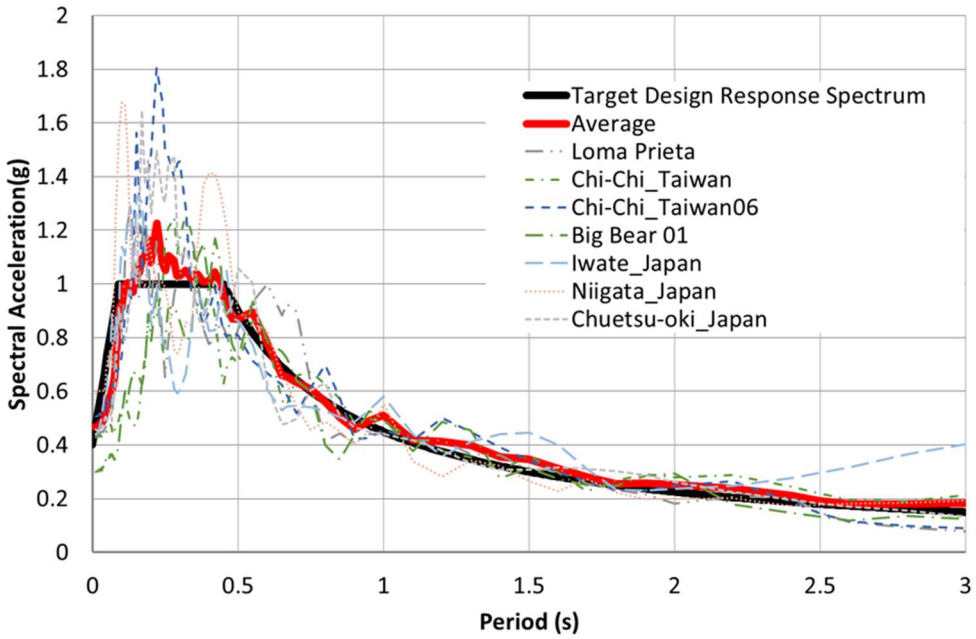

Figure 6.1. The target design response spectrum and the average of the response spectra of the selected ground motions

6.3 Nonlinear Structural Modeling of the Bridges

To investigate the effect of girder spacing on the seismic performance of bridges for various structural properties, their nonlinear structural models are built separately for longitudinal and transverse direction analyses with different modeling approaches for the abutments. The main reason for using separate models for the longitudinal and transverse direction analyses of the bridges is to reduce the run-time by employing a smaller degrees of freedom in each direction. Various modelling features such as compression only springs, gap and dashpot elements as well as Takeda nonlinear hysteretic link element facilitated the simulation of complex behavioral types such as behavior of backfill and foundation soil, impact between the deck and abutment back-wall and inelastic hysteretic behavior of the pier columns. The structural model of the bridges is shown in Fig. 6.2. In the following subsections, the details of the nonlinear structural model are presented.

6.3.1 Modeling of the Abutments in the Longitudinal Direction

The abutment model is shown in Fig. 6.3. It is composed of two parts; (i) the part that simulates the interaction between the bridge deck, back-wall and backfill upon impact of the deck with the abutment back-wall and (ii) the part that simulates the interaction between the bridge deck, bearings and the abutment-backfill system at the seat level.

For part (i) of the abutment model, the procedure defined in the CALTRANS Seismic Design Criteria (2019) is followed to model the structure-abutment-backfill interaction upon impact of the deck with the abutment back-wall. A bilinear force-deformation relationship is defined in CALTRANS Seismic Design Criteria (2019) to simulate the force-deformation behavior of the abutment in the case of impact of the superstructure with the abutment back wall. The ultimate passive capacity of the abutment, F_{abut} and its longitudinal stiffness, K_{abut} are calculated using the equations given below:

$$F_{abut} = w_{abut}\left(\frac{5.5h_{abut}^{2.5}}{1+2.37h_{abut}}\right) \quad (11)$$

$$K_{abut} = w_{abut}(5.5h_{abut} + 20) \quad (12)$$

Where w_{abut} is the abutment width, h_{abut} is the height of the back wall. Note that, Equations 11 and 12 are given in imperial units.

A dashpot element is introduced to the seismic model at the abutment locations to simulate the energy dissipation in the case of pounding of the deck with the abutment. The damping coefficient (c_k) is calculated using the equations proposed by Desroches and Muthukumar (2004).

$$c_k = 2\xi\sqrt{k_k\left(\frac{m_1 m_2}{m_1+m_2}\right)} \quad (13)$$

$$\xi = -\frac{\ln}{\sqrt{\pi^2+(\ln e)^2}} \quad (14)$$

In the above equations, m_1 and m_2 is the masses of the abutment and the superstructure respectively, e is the coefficient of restitution (assumed as 0.8), and k_k is the spring stiffness taken as 4.38×10^6 kN/m.

Since, both dashpot element and the spring defined in CALTRANS (2019) is engaged only when superstructure pounds the abutment, a gap element, having a width equal to that of the expansion joint is introduced to the structural model.

For part (ii) of the abutment model, a spring with different stiffnesses in tension and compression is used to define the force-deformation behavior of the abutment-backfill system. To obtain the stiffness of the abutment-backfill system for the cases where the abutment moves away (active or tension) or pushes against the backfill (passive or compression), A full 2D model of the abutment is built as shown in Fig. 6.4. where the abutment-backfill interaction is implemented in the structural model using compression-only horizontal springs. The mass of the abutment is also defined as lumped masses at the nodes. The spring constants for the backfill are then calculated using the relationship proposed by Dicleli and Mansour (2003) as follows;

$$k_{sh} = \left(\frac{14500}{H}\right) z \quad (15)$$

where, H is the abutment height, z is the depth measured from the abutment top and k_{sh} is the horizontal subgrade constant. The compression only behavior of the backfill is simulated by implementing gap elements between the abutment and the backfill springs. The abutment footing-foundation soil interaction is modeled by three translational and three rotational springs as defined by (Dobry and Gazetas (1986). Next pushover analyses of the abutment-backfill model are performed in the active and passive directions to define the stiffness of the abutment-backfill system. The abutment-backfill spring is then supported by a roller at the end and connected to another spring representing the stiffness of the elastomeric bearings. An equivalent mass is imposed over the roller support to define the dynamic behavior of the abutment for the stages where the deck does not impact the abutment back-wall. To

obtain the magnitude of this equivalent mass, only the linear response of the abutment-backfill system is considered (when the deck does not impact the abutment back-wall, the behavior of the abutment-backfill system is nearly linear). Next NTHA of the 2D abutment model defined above is conducted, using the previously selected seven ground motions. In each ground motion, the maximum displacement of the node where the superstructure of the bridge is assumed to be connected to the abutment is determined. Then, the same ground motions are applied to a single degree of freedom system attached to a mass (the abutment-backfill spring supported by a roller at the end). An equivalent mass is found using trial and error approach which has average maximum displacement identical to that of the monitored node of the abutment. Similar average maximum displacement is achieved at an equivalent mass, which is %25 of the actual abutment mass.

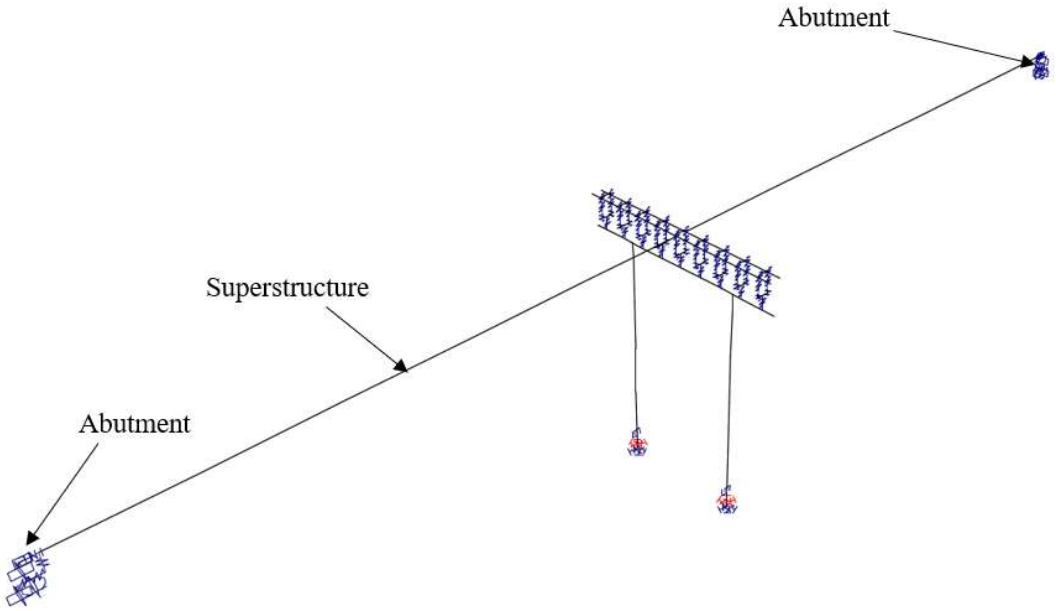

Figure 6.2. Overall view of the longitudinal model

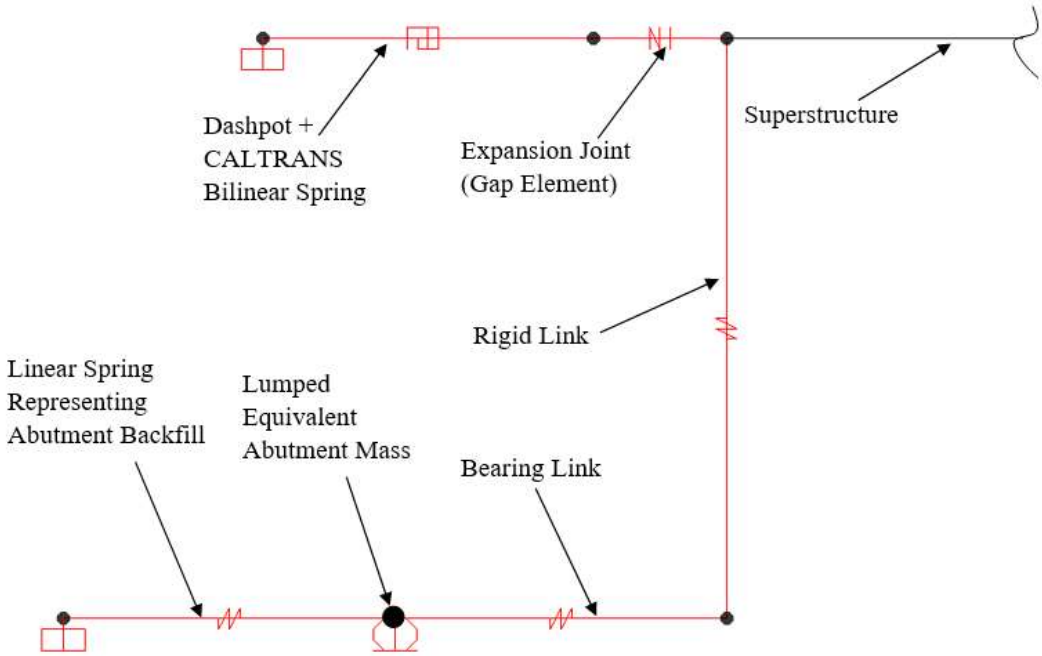

Figure 6.3. Detailed view of the abutment in the longitudinal model

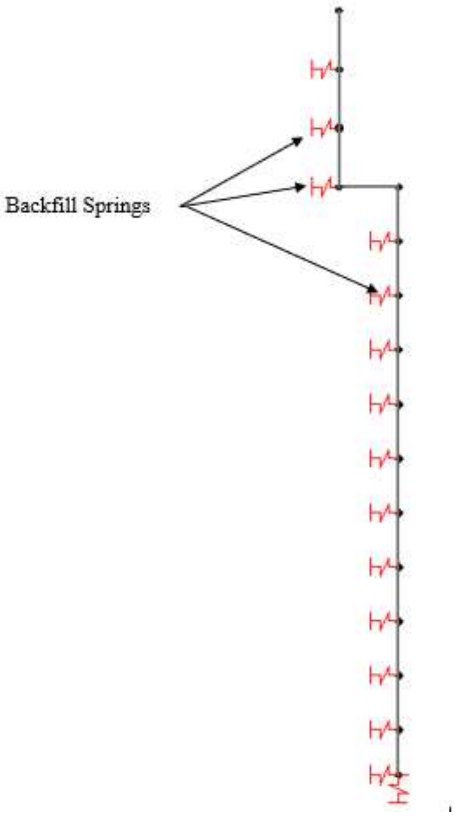

Figure 6.4. 2D abutment model

6.3.2 Modeling of the Abutments in the Transverse Direction

In the transverse direction, abutment wall, wing walls and abutment foundation is idealized using frame elements, having equivalent line masses. The backfill response is simulated using horizontal springs as defined in Equation 15. The interaction between soil and abutment foundation is modeled using translational and rotational springs (Dobry and Gazetas, 1986).

To reflect the friction between the abutment wall and the backfill, in the case of shear deformation under transverse seismic loading, a simple elastic approach is adopted. In this approach, it is assumed that only the portion of the backfill between the wing walls will deform under transverse seismic loading. Accordingly, the shear stiffness, k_{sh} is given as:

$$k_{sh} = \frac{GBH}{L_w} \tag{16}$$

where B is the width between two wing walls, H is the abutment height, L_w is the length of the wing wall and G is the shear deformation modulus of the backfill.

The ultimate capacity of the shear resistance of the backfill (V_u) is calculated as:

$$V_u = \mu F_0 \tag{17}$$

where μ is the coefficient of friction, calculated as:

$$\mu = tan\phi \tag{18}$$

and F_0, the at rest earth pressure, is calculated as:

$$F_0 = \frac{1}{2}\gamma H^2 B K_0 \tag{19}$$

In Equation 18, Φ is the friction angle between backfill and the abutment wall. In Equation 19, γ is the unit weight and K_0 is the at rest pressure coefficient of the backfill.

Details of the model of the abutments is illustrated in Figure 6.4.

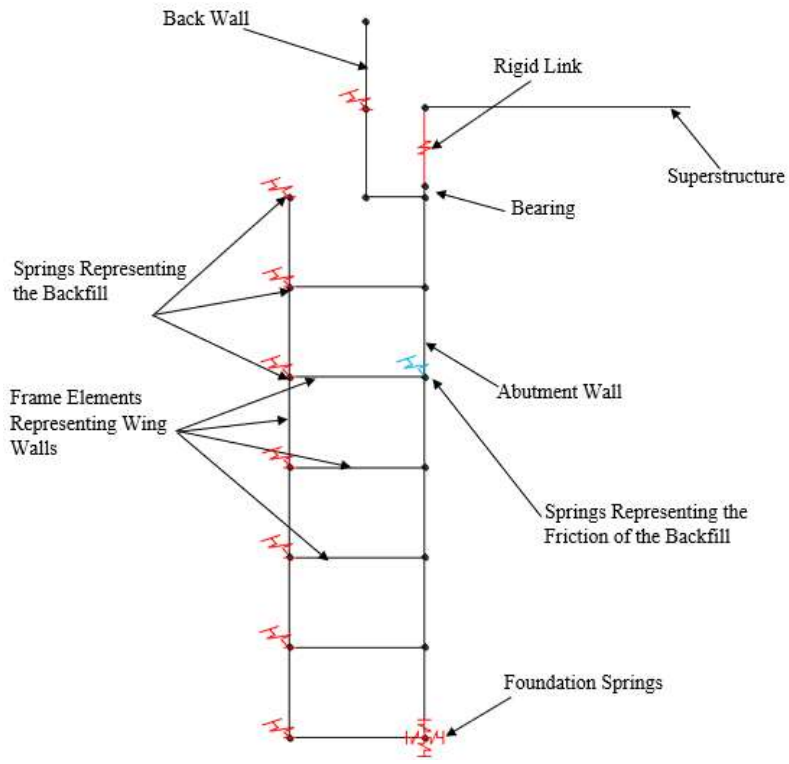

Figure 6.5. Detail view of the abutment in the transverse model

6.3.3 Modeling of the Piers

To determine the non-linear behavior of the reinforced concrete circular columns used in this study, first, the moment-curvature relationships of the columns under dead load are obtained using the Section Designer module of SAP2000. The hysteretic behavior of the reinforced concrete members is introduced to the structural models using non-linear plastic links at the anticipated plastic hinging locations in the columns. The hysteresis model proposed by Takeda et. al. (1970) is adopted in this research study as it is widely accepted for defining non-linear hysteresis behavior of reinforced concrete members (Alkhrdaji and Silva, 2000). Footing-soil interaction at the piers are idealized using translational and rotational springs (Dobry and Gazetas, 1986).

6.4 Discussion of the Seismic Performance Analysis Results

6.4.1 Girder Spacing versus Peak Ground Acceleration

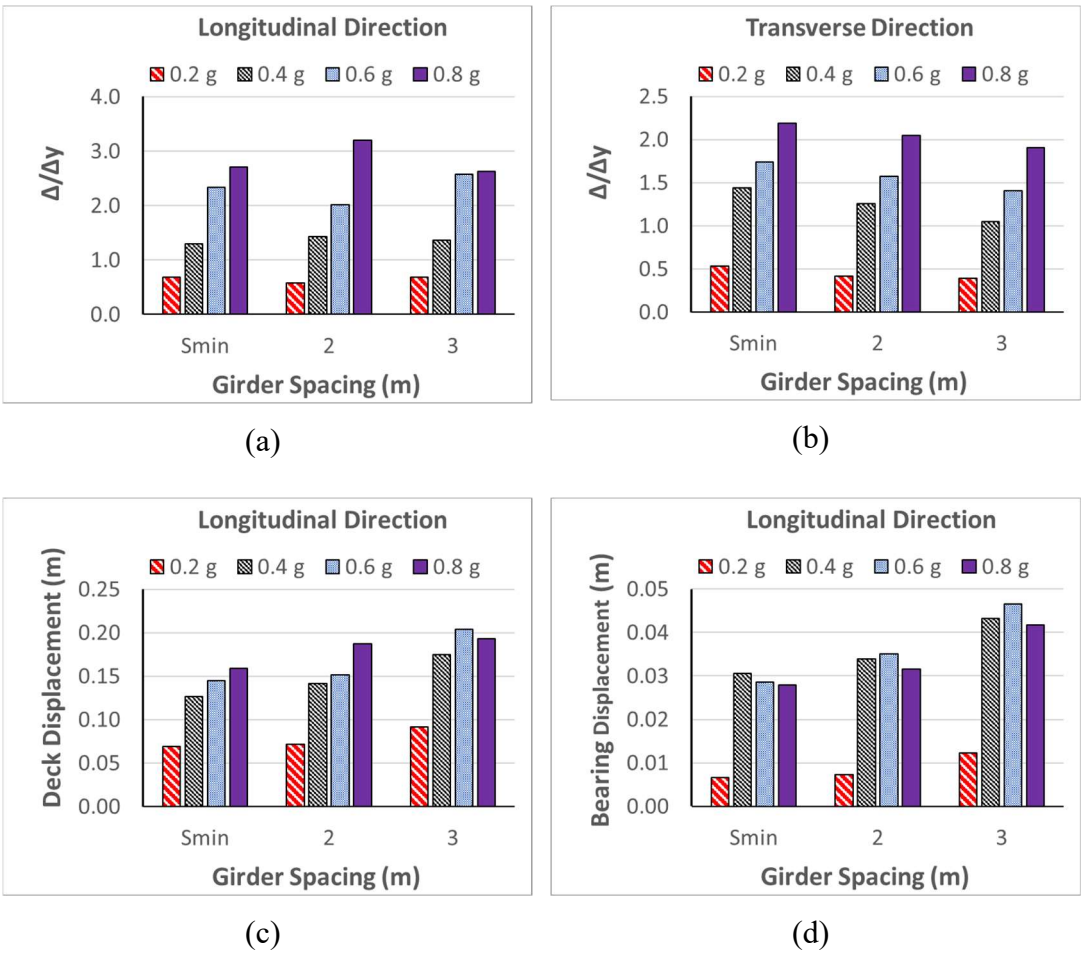

Figure 6.6. Ductility ratio (Δ/Δ_y) versus girder spacing (a) in the longitudinal direction, (b) in the transverse direction, (c) deck displacement in the longitudinal direction versus girder spacing, (d) bearing displacement in the longitudinal direction for different values of PGA

In Figure 6.5., the relationship between the ductility ratios (Δ/Δ_y) as well as deck and bearing displacements versus girder spacing for the different cases of PGA are given in a bar chart form. As observed from the figure, ductility ratios increase as the girder spacing increases regardless of the peak ground acceleration in the longitudinal direction of the bridge. For the cases of ductility ratios, deck displacements and

bearing displacements in the longitudinal direction, mixed results are obtained. Note that, as the girder spacing increases, total stiffness of the bridge decreases due to the lower number of bearings on the pier. The total mass of the superstructure also decreases; however, the decrease in the total mass of the structure is limited, due to the presence of slab in every case and increased girder dimensions as the girder spacing increases. The reduction of the bridge stiffness is more pronounced, compared to the reduction in the superstructure mass, resulting in higher ductility ratios (lower seismic performances) in the case of increased girder spacing in the longitudinal direction in some bridges. Moreover, since the cross-sectional dimensions, reinforcement of the columns and tributary mass on the columns are different in each case, columns have varying moment-curvature relationship and hence, all the columns have different displacement capacity before yielding. This may be the reason of obtaining mixed results for ductility ratios, deck and relative bearing displacements. The effect of the column on the seismic performance will be discussed in more detail in the upcoming sections. In the transverse direction, the stiffness of the frame system, formed by two columns and the cap beam may govern the seismic behavior, rather than the stiffness of the elastomeric bearings because, relative displacement of the elastomeric bearings are constrained in the transverse direction. Column cross-sectional diameter increases as the girder spacing decreases, increasing the stiffness of the frame system. However, in the transverse direction, the decrease in the superstructure mass may have more impact on the overall behavior of the bridge, resulting in an improvement in the seismic performance as the girder spacing increases.

6.4.2 Girder Spacing versus Span Length

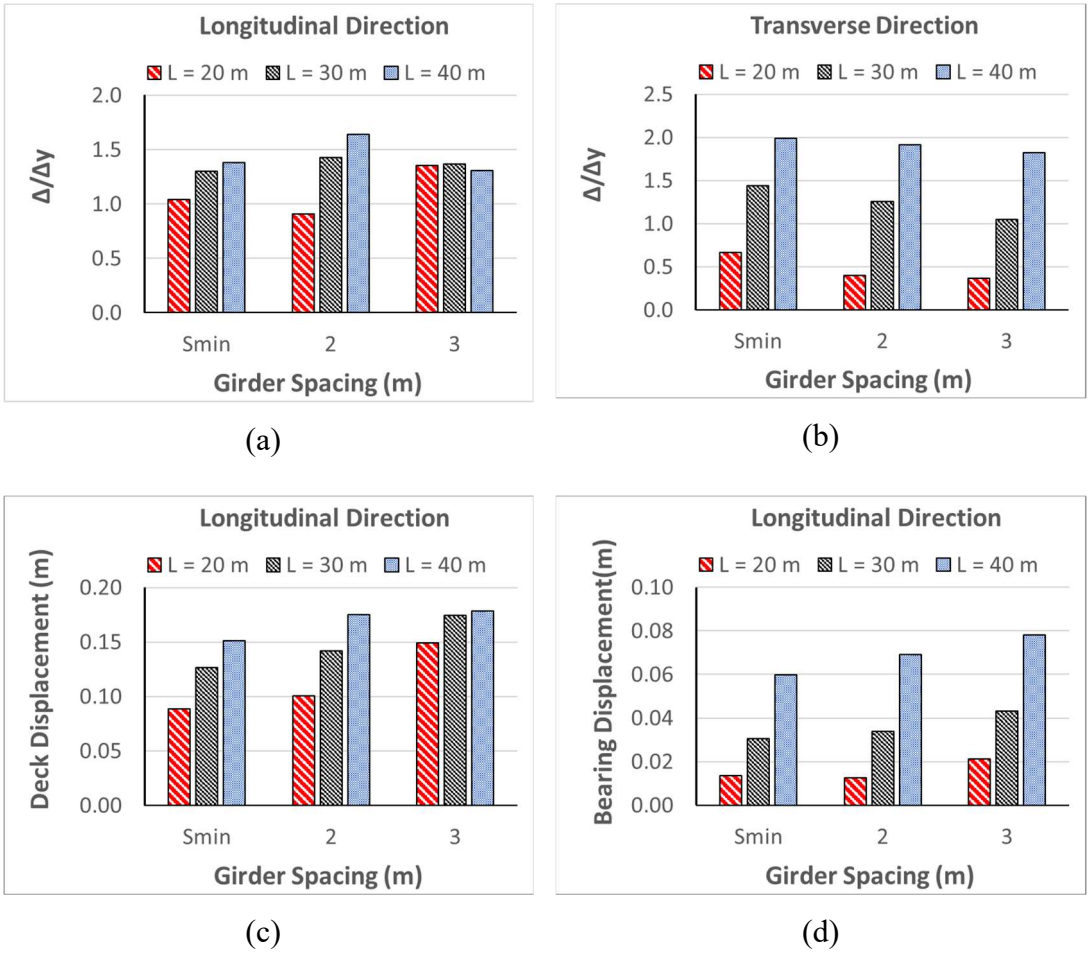

Figure 6.7. Ductility ratio (Δ/Δ_y) versus girder spacing (a) in the longitudinal direction, (b) in the transverse direction, (c) deck displacement in the longitudinal direction versus girder spacing, (d) bearing displacement in the longitudinal direction for different values of span lengths

In Figure 6.6., the relationship between the ductility ratios (Δ/Δ_y), deck and bearing displacement versus girder spacing for the different values of span lengths are represented. In the longitudinal direction, the variation in the ductility ratios are not proportional to the change in the girder spacing and span length. As the span length increases, the mass of the superstructure increases, leading to amplified seismic forces in the columns and consequently increasing the selected column diameter. This results in different yield capacity values among each considered case. As

described in the previous section, the decrease in the stiffness is more severe than the decrease in the superstructure mass as the girder spacing increases. Since the parameters affecting the displacements under seismic loading show a large variation, ductility ratios are not consistent with the change in girder spacing in the longitudinal direction. In the transverse direction, more meaningful variation is achieved among each considered case. As in the previous case where different values of PGA are compared, decrease in the mass of the superstructure leads to better seismic performance. Deck and relative bearing displacements tend to increase with the increase in the girder spacing. This may be due to selecting smaller cross-sectional diameter for the columns as the girder spacing increases.

6.4.3 Girder Spacing versus Number of Spans

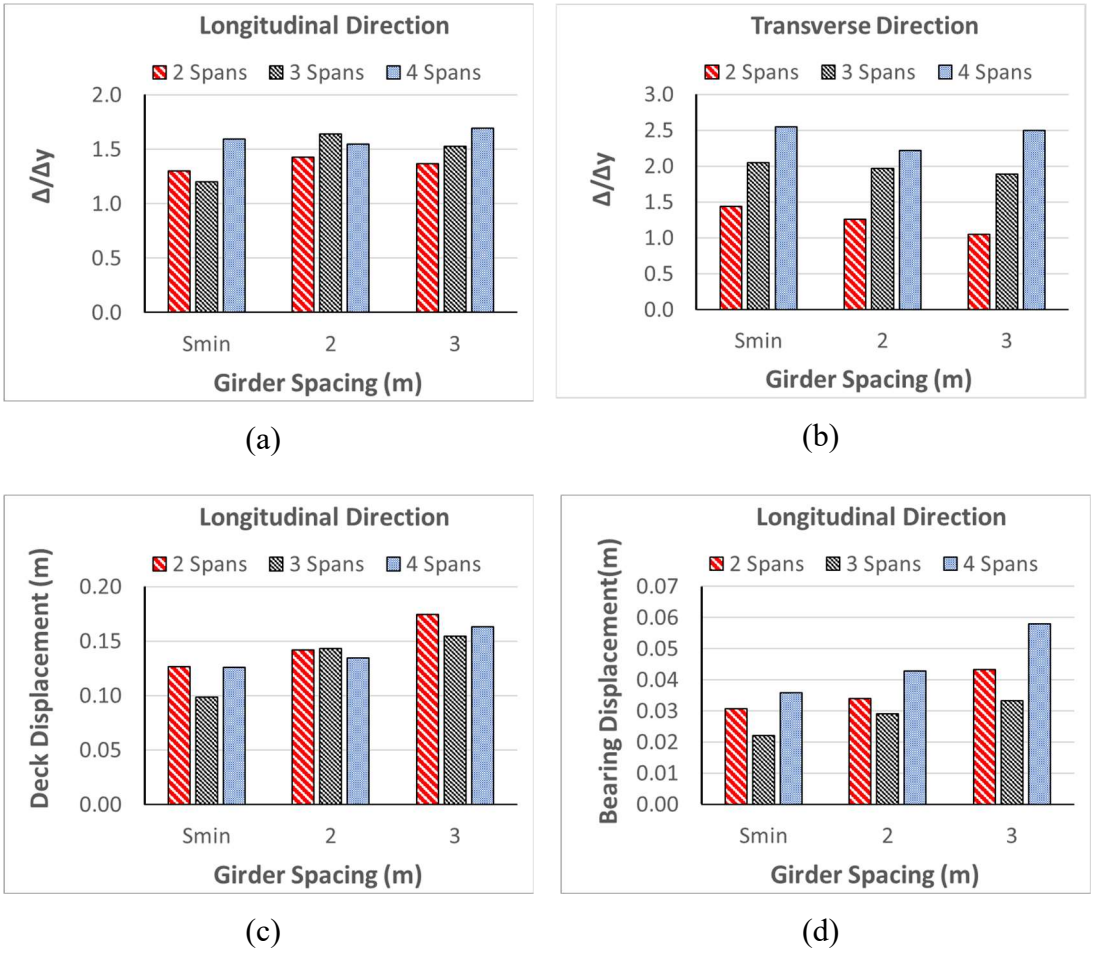

Figure 6.8. Ductility ratio (Δ/Δ_y) versus girder spacing (a) in the longitudinal direction, (b) in the transverse direction, (c) deck displacement in the longitudinal direction versus girder spacing, (d) bearing displacement in the longitudinal direction for different values of number of spans

In Figure 6.7., the relationship between the ductility ratios (Δ/Δ_y), deck and bearing displacement versus girder spacing for the different number of spans are represented. As seen from the above figure, ductility ratios, deck and relative displacements are not in a trend among both different values of number of spans and girder spacing. As the number of spans are increasing, the column diameter also increases due to seismic loading in transverse direction. This leads to selection of columns having

different cross-sectional diameter among the cases of 2, 3 and 4 spans. Therefore, unpredictable variation among monitored seismic behavior is observed for each considered case. Contrary to the case where different values of span lengths are compared, tributary mass on the pier is same for 2, 3 and 4 span cases, however in each case, column cross-sectional diameter is different, further adding unpredictability to the comparison.

6.4.4 Girder Spacing versus Column Height

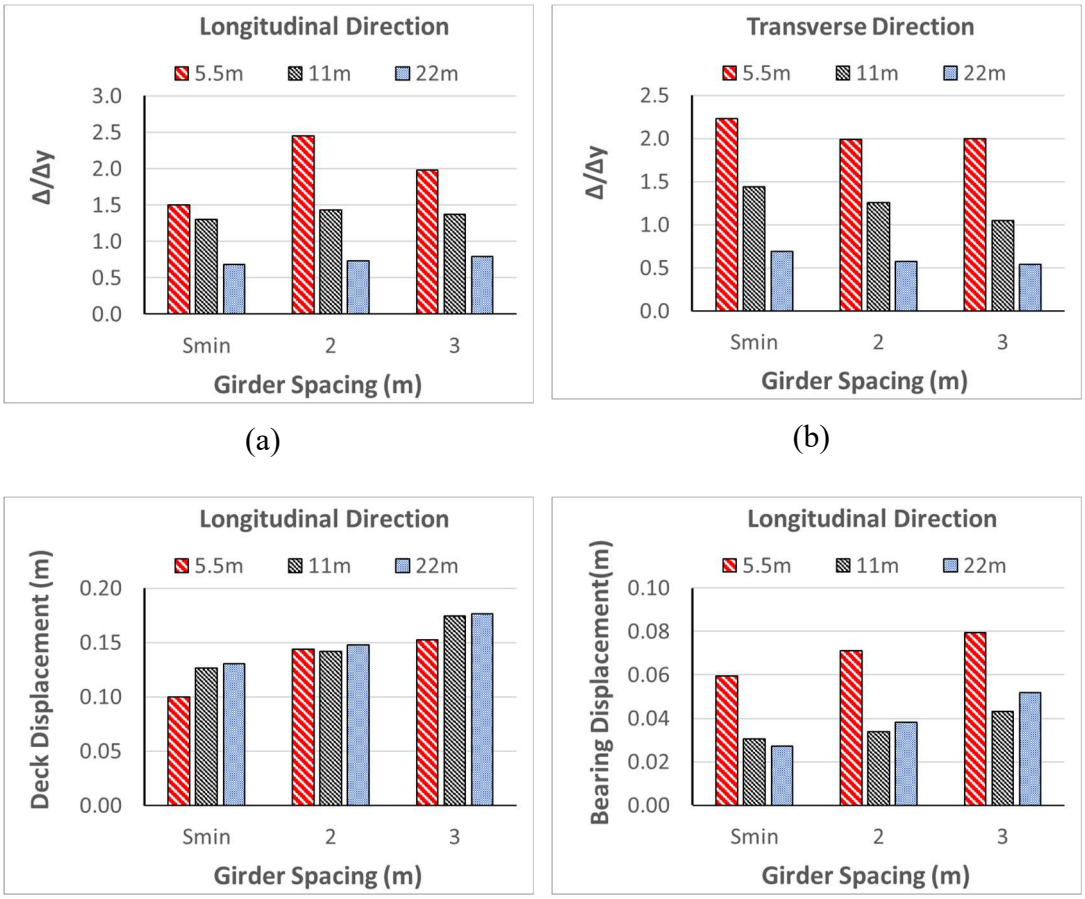

(a) (b)

(c) (d)

Figure 6.9. Ductility ratio (Δ/Δ_y) versus girder spacing (a) in the longitudinal direction, (b) in the transverse direction, (c) deck displacement in the longitudinal direction versus girder spacing, (d) bearing displacement in the longitudinal direction for different values of column heights

In Figure 6.8., the relationship between the ductility ratios (Δ/Δ_y), deck and bearing displacement versus girder spacing for different column heights are represented. As discussed earlier, due to considerable variation in parameters affecting the seismic behavior such as superstructure mass, bearing stiffness, column section, mixed results are obtained for ductility ratios, deck and relative bearing displacements. In the transverse direction, ductility ratios are in a decreasing trend, due to reasons described in earlier sections.

6.4.5 Additional Performance Analyses for Further Discussion

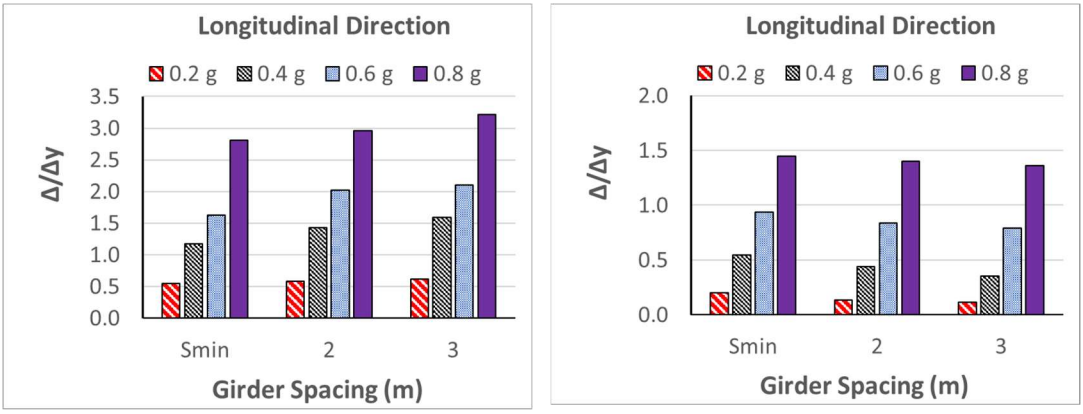

(a) (b)

Figure 6.10. Girder spacing versus peak ground acceleration for (a) tension-controlled column section (b) compression-controlled column section

To further observe the effect of the columns on the seismic performance, additional seismic performance analyses are conducted. For this purpose, two additional analyses sets are built. In the first set (Figure 6.9. (a)), for each girder spacing considered, the same cross-section for columns and elastomeric bearings having the same stiffness are used. In the second set (Figure 6.9. (b)) same column cross-sections are used for each considered girder spacing, however, they are modified so that, column cross-sections are compression controlled (the axial force is higher so that the column behavior is controlled more by the axial load within the region above the balance point). As observed from the figure, as the girder spacing increases, the

ductility ratios also increase for the first set. For the second set, where the column cross-sections are compression-controlled, an opposite relationship is observed. In a section that behaves below the balance point (flexure dominant behavior), as in the case of the first set, as the axial load on the column decreases, moment capacity of the column also decreases. However, in a compression-controlled section, decrease in the axial load on the column increases the moment capacity. This relationship is illustrated schematically in the interaction diagrams in Figure 6.10. Since design codes require flexure-dominant sections, as considered in this study, increasing the girder spacing that produces smaller axial load on the column, has an adverse effect on the seismic performance of the bridge.

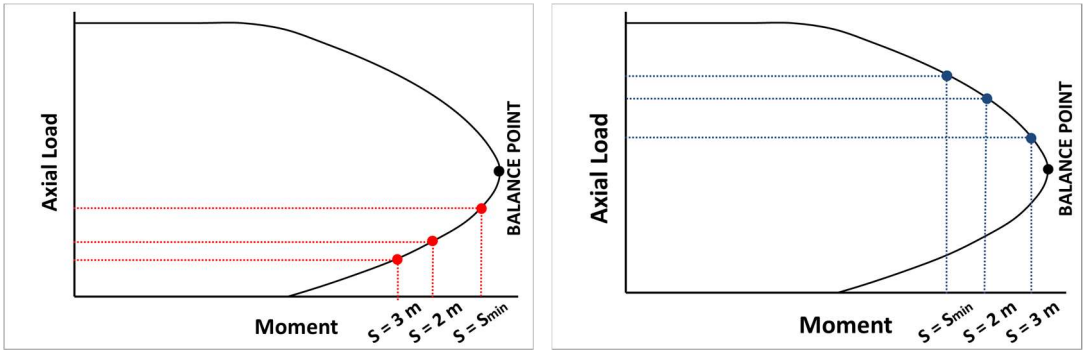

(a) (b)

Figure 6.11. Column interaction diagrams for (a) tension-controlled section, (b) compression-controlled section failure

CHAPTER 7

CONCLUSIONS

The major conclusion to be drawn from this research study is that the current bridge construction practice in Turkey needs to be revised as urgently as possible. Having the prestressed girders placed with minimum gap has no real benefit, compared to placing the girders with spacing. Considering the number of bridges constructed in Turkey each year, current practice causes a huge amount of public funds to be wasted. Therefore, revising the current bridge construction approach will lead to significant saving on highway construction budgets.

Another conclusion obtained by the analyses conducted herein showed that bridge construction costs are shown to considerably reduce, up to 22%, when the girder spacing is increased. With larger number of spans, the drop in the bridge construction cost is also higher. It is anticipated that the drop in the construction costs goes down further in the cases of longer and wider bridges, since the main contribution to construction cost reduction comes from the number of prestressed girders used in the construction of the bridge and their cost

Moreover, increasing the girder spacing, thus decreasing the number of girders results a lighter superstructure. This leads to a decreased dead and design seismic forces transmitted to the substructure from the superstructure. Therefore, having less girders in the superstructure also leads to savings for the cost of the substructure.

In addition to the above findings, for softer soils, the effect of the girder spacing on the construction costs decreases, since the contribution to the overall construction costs from the substructure considerably increases.

Seismic performance analyses revealed that, increasing the girder spacing does not affect the seismic performance considerably. While seismic performance may benefit from having reduced superstructure mass as the girder spacing increases, decreased column dimensions and bearing stiffnesses may affect the seismic

performance negatively. Overall, nearly similar levels of seismic performance is observed for each considered case of girder spacing

REFERENCES

Adibaskoro, T., & Suarjana, M. (2019). Prestressed Concrete I-Girder Optimization via Genetic Algorithm. Journal of Engineering and Technological Sciences, 51(2), 170-183.

Ahsan, R., Rana, S., & Ghani, S. N. (2012). Cost optimum design of posttensioned I-girder bridge using global optimization algorithm. Journal of Structural Engineering, 138(2), 273-284.

Alkhrdaji, T., & Silva, P. (2008). Seismic Strengthening of Concrete Buildings Using FRP Composites. American Concrete Institute.

American Association of State Highway and Transportation Officials (AASHTO). (2017). AASHTO LRFD Bridge Design Specifications (8th Edition). American Association of State Highway and Transportation Officials (AASHTO).

Aydın, Z., & Ayvaz, Y. (2013). Overall cost optimization of prestressed concrete bridge using genetic algorithm. KSCE Journal of Civil Engineering, 17(4), 769-776.

Batikha, M., Al Ani, O., & Elhag, T. (2017). The effect of span length and girder type on bridge costs. In MATEC Web of Conferences (Vol. 120, p. 08009). EDP Sciences.

Caltrans, S. D. C. (2019). Caltrans seismic design criteria version 2.0. California Department of Transportation, Sacramento, CA.

Computers and Structures, Inc. (2009). CSI analysis reference manual for SAP2000.

DesRoches, R., & Muthukumar, S. (2004). Implications of seismic pounding on the longitudinal response of multi-span bridges—an analytical perspective. Earthquake Engineering and Engineering Vibration, 3(1), 57-65.

Dicleli, M., & Mansour, M. Y. (2003). Seismic retrofitting of highway bridges in Illinois using friction pendulum seismic isolation bearings and modeling procedures. Engineering Structures, 25(9), 1139-1156.Dobry, R., & Gazetas, G. (1986). Dynamic response of arbitrarily shaped foundations. Journal of geotechnical engineering, 112(2), 109-135.

Federal Emergency Management Agency. (2000). Prestandard and commentary for the seismic rehabilitation of buildings. American Society of Civil Engineers (ASCE).

Kavazanjian Jr, E., Matasovic, N., Hadj-Hamou, T., & Sabatini, P. J. (1997). Geotechnical Engineering Circular No. 3: Design Guidance. Geotechnical Earthquake Engineering for Highways. Volume I-Design Principles (No. Report No: FHWA-SA-97-076).

Lounis, Z., & Cohn, M. Z. (1993). Optimization of precast prestressed concrete bridge girder systems. PCI Journal, 38(4), 60-78.

Rabbat, B. G., & Russell, H. G. (1984). Proposed replacement of AASHTO girders with new optimized sections. Transportation Research Record, 950, 85-92.

Rana, S., Islam, N., Ahsan, R., & Ghani, S. N. (2013). Application of evolutionary operation to the minimum cost design of continuous prestressed concrete bridge structure. Engineering structures, 46, 38-48.

Sirca Jr, G. F., & Adeli, H. (2005). Cost optimization of prestressed concrete bridges. Journal of Structural Engineering, 131(3), 380-388.

Takeda, T., Sozen, M. A., & Nielsen, N. N. (1970). Reinforced concrete response to simulated earthquakes. Journal of the Structural Division, 96(12), 2557-2573.

Yu, C. H., Gupta, N. D., & Paul, H. (1986). Optimization of prestressed concrete bridge girders. Engineering optimization, 10(1), 13-24.